Università degli Studi di Milano

FACOLTÀ DI SCIENZE E TECNOLOGIE
Bachelor of Science in Physics

Degree thesis

Potentials and Densities from the Solution of the Nuclear Inverse Kohn-Sham Problem

Candidate:
Paolo Brandolini
Student Number 697399

Supervisor:
Prof. Gianluca Colò

Advisor:
Dott. Xavier Roca Maza

Academic year 2017-2018

Dedication

for my Mom

for my Dad

for my family

for my friends

‘The most exciting phrase to hear in science, the one that heralds the most discoveries, is not ”Eureka!” (I found it!) but ”That’s funny...”

Isaac Asimov

Contents

List of Tables

List of Figures

Constants and notations

Proton mass ($m_p c^2$)	938.38 MeV
Neutron mass ($m_n c^2$)	939.56 MeV
Proton radius r_p	0.8751 fm
Nuclear surface thickness a	0.67 fm
Elementary charge q_e	1.43 $MeV \cdot fm$
Laplacian operator	$\bigtriangledown^2$
Planck's constant ($\hbar c$)	197.32 $MeV \cdot fm$

Source: https://physics.nist.gov/cuu/Constants/

Chapter 1

Introduction

The nucleus is a self-contained system of elementary particles (protons and neutrons), which can in turn give rise to much more complex particle systems, such as neutron stars. Understanding the fundamental structure of nulear matter is not simple, mainly because the dimensions of its constituents are very small. Just think that the diameter of an average nucleus is about $10^{-12}cm$ and that the average distance between two nucleons is about $2 \cdot 10^{-13}cm$.

The research in the nuclear field, offers a varied choice of possibilities for investigation. Many steps forward have been made in these decades, but the road that leads to a deeper knowledge of the structure of the nucleus is still long. One of the major avenues is aimed at understanding the nuclear forces that come into play in a system of interacting nucleons. Even today, we do not know an exact analytical form of nuclear interaction, since being a *short-range* force (about $1fm$), it is difficult to probe rigorously. Over the years, physicists have developed mathematical models to reproduce and predict the dynamics that take place in a nuclear system. Based on the experimental evidence, we have moved from the roughest liquid drop model to the most complete mean field models. The latter approximate the nucleus as a system of N non-interacting nucleons but that are experienced by the average field generated by the other $N-1$ nucleons and are able to describe a good part of the nuclear phenomena. The *Hartree-Fock* (HF) model is the most widely used tool in the nuclear environment. It consists of an iterative and self-consistent numerical method that can produce an effective potential that characterizes a given physical system. The prediction takes place starting from specific fermionic interactions to reproduce certain observables of the system preserving its symmetry. Just the strong dependence on specific parametrizations (those of *Skyrme* and *Gogny* are an example), make the HF method limited.

An alternative approach that allows the study of physical systems without requiring specific inputs

adapted to the individual case under study is represented by the use of *Density Functional Theory* (DFT). The theory is based on the biunivocal relationship between potential and fermionic density, maintaining a universal character that is not present in the HF theory. Originally enveloped in the atomic environment by *P. Hohenberg* and *W. Kohn*, the DFT finds its practical application through the *Kohn-Sham* equations, representing the *direct problem*.

The entry of the DFT in nuclear physics took place in previous years through the study of the direct problem, documented in the literature, without ever facing the inverse formulation. *Inverse problems* are common in science and take on particular importance in quantum mechanics. Much of what we know about the structure of matter came from scattering experiments, which can be described mathematically as inverse problems.

The present thesis project, aims to apply the formulation of the inverse problem of Kohn-Sham in the nuclear field, attempting to fill a gap in the literature in this context. Through the DFT theory and the solution of the Kohn-Sham equations, a mathematical model is developed that generates a potential that is more similar to the real one, starting from experimental densities. In particular, the inversion algorithm proposed by *R. van Leeuwen* and *E. J. Baerends* and studied with the intent of understanding its efficiency and limitations. The results obtained are discussed with reference to what is already known and compared with the solution of the inverse problem obtained by two other methods: the already mentioned HF method and the Constraint Variational method (CV), also formulated on the DFT theory. Attention is focused on three nuclei in particular, the ^{16}O, the ^{40}Ca and the ^{208}Pb. The choice of these nuclei is justified by the fact that they are doubly magical nuclei, with spherical symmetry and equipped with closed shells. In this way, the physical system under examination can be simplified as much as necessary to avoid unwanted effects (such as the effect of *pairing*) and to better appreciate the operation of the inversion method. In the following pages of the present thesis, the basic elements of nuclear physics are introduced, such as the constituents and the known phenomenological models, and the mathematical setting of the DFT is presented in the following sections. Finally, after describing the model developed, the results obtained are appropriately commented on.

Chapter 2

Nuclear systems

In this first chapter, a brief reference to the fundamentals of nuclear physics is given describing the constituents of the nucleus and their main properties. The theoretical tools are described in a completely general way and giving more space to the importance they assume in the nuclear domain, such as the use of a *shell model* that allows to simplify the study of nuclear systems making it easier to calculate the main physical quantities (eigenfunctions, energies, probability density, etc ...) that can be compared with the known experimental evidences. Only in the successive phases, after introducing the Functional Density Theory, will we proceed to a more specific treatment.

2.0.1 Costituents, forces and properties

The charge of the nucleus is equal to Ze, where Z is atomic number and identifies the number of *protons*, while e is the value of eletronic charge.

Another component of the nucleus is the *neutron*, electrically neutral and with a mass approximately to that of the proton. Each nuclear species contains $N = A - Z$ neutrons. Neutrons and protons are called *nucleons*.

With the symbol A, we identify the mass number that is defined as the total number of costituents (protons plus neutrons). $A > Z$

A specific nuclear species, or *nuclide*, is represented as ${}^{A}X$, where X is the chemical symbol. Specifically, nuclei with the same value of Z but different value of N are called *isotopes*, nuclei with the same N but different Z are called *isotones* and finally, nuclei with the same value of A are called *isobars*. Nuclei with certain values of A and Z can be in excited states, *isomers* or *resonances*, decaying to the ground state

emitting electromagnetic radiation ($\gamma\ rays$).

The mass of a nucleus is less than the sum of the masses of its constituents

$$M(A,Z) < Zm_p + (A-Z)m_n, \tag{2.1}$$

where with m_p and m_n we indicate the mass of protons and neutrons respectively. This property guarantees the stability of a nucleus. The difference in mass is due to the binding energy due to nuclear forces

$$E_{binding}/c^2 = M(A,Z) - Zm_p - (A-Z)m_n. \tag{2.2}$$

The inner part of a nucleus has a constant density $n_0 \approx 0.16\ fm^{-1}$ and the nuclear surface has a thickness of $\approx 0.6\ fm$.

The cohesion of nucleons to form the nucleus is induced by the nuclear force that manifests itself by means of the nucleon-nucleon interaction, more specifically in the *strong interaction* mediated by the exchange of pions and mesons between nucleons. Its nature is purely attractive for distances close to $1\ fm$ and decays rapidly to reach negligible values at a distance of about $2.5\ fm$. At distances less than $0.4\ fm$, the strong interaction assumes repulsive behavior.

There are particular values of N and Z for which the nuclei are expected to have a relatively high binding energy. These highly bound states occur when N and Z assume certain values called "*magic numbers*". The magic numbers observed so far have values

$$2, 8, 20, 28, 50, 82, 126. \tag{2.3}$$

Some nuclei have both Z and N as magic numbers and are called "*doubly magical*", showing an even stronger bound energy. An example is the $^{208}_{82}Pb$ ($Z = 82, N = 126$).

2.0.2 Nuclear mean-field and Hartree-Fock method

The study of nuclear systems takes place through the use of mathematical models that can be *ab initio* or macroscopic, like as the *liquid drop model*.

The first are based on the nucleon-nucleon potential and reproduce with good accuracy the experimental

data related to the scattering between nucleons, but are so far unsuitable - for example - for an estimate of the saturation point (defined later in the discussion), as they are not exploitable for the study of many-body systems.

During the first years of study of the atomic nucleus, precisely because of its conformation characterized by strongly interacting nucleons and confined in a restricted region, the analogy between the nuclear system and that related to a charged liquid drop seemed more obvious. In fact, the liquid drop model is based on the following hypotheses:

- The energy of interaction between nucleons is independent of the type and number of nucleons;
- The interaction is attractive at distances around R_{int} (as for the drops of a liquid, whose molecules that compose them have dipole-dipole interactions);
- The interaction is repulsive at distances $r << R_{int}$;
- The binding energy of the nucleus is proportional to the number of nucleons.

and from it comes the well-known semi-empirical equation of *Bethe-Weizsäcker*

$$E_{binding}(A,Z) = -a_v A + a_s A^{\frac{2}{3}} + a_c \frac{Z(Z-1)}{A^{\frac{1}{3}}} + a_{sym}\frac{(A-2Z)^2}{A} \pm \frac{\delta}{A^{\frac{1}{3}}}, \tag{2.4}$$

whose terms are respectively the volume, surface, Coulomb, symmetry and pairing terms.

A system with the same number of protons and neutrons and having an equilibrium density of n_0 is comparable to a piece of symmetric nuclear matter (SNM). By focusing on the case of uniform SNM, the terms of the (2.4) vanish except for the volume-dependent term. Then, the particle energy in the case of equilibrium density, is equal to $E_0 = -16\ MeV$. This is defined as the *saturation point* in SNM approximation.

Macroscopic models such as liquid drop model, on the other hand, are limited to reproducing only the average properties of the systems under study and are based only on phenomenological considerations. Furthermore, they do not explain the existence of nuclear magic numbers and other the shell model properties. A middle way between these two types of model is represented by the nuclear *mean-field model*.

Considering a nucleon as a point particle without an internal structure, the many-body theory shows how difficult it is to solve the Schrödinger equation for nuclear systems characterized by a value of $A > 10$. In order to circumvent this limitation, the practice of approximating a strongly interacting particle system

with a system of A almost non-interacting particles has advanced in the years of study. The remaining interactions, residual interactions, are treated by perturbation theory.

Let H be the nuclear Hamiltonian of a many-body system made up of a kinetic part and a potential part as follows

$$H = T + V = \sum_{i=1}^{A} t(r_i) + \sum_{i,j=1;i<j}^{A} v(r_i, r_j) = \sum_{i=1}^{A} \frac{-\hbar^2}{2m_N} \nabla_i^2 + \sum_{i,j=1;i<j}^{A} v(r_i, r_j), \tag{2.5}$$

where with m_N the identified proton and neutron masses are identified ($m_N c^2 = 940 MeV$) and r_i denotes the nucleon coordinate i. A potential single-particle energy can be added and subtracted

$$H = [T + \sum_{i=1}^{A} v(r_i)] + [V - \sum_{i=1}^{A} v(r_i)] = H_{MF} + V_{RES}, \tag{2.6}$$

where

$$H_{MF} = T + \sum_{i=1}^{A} v(r_i) \equiv T + V_{MF} = \sum_{i=1}^{A} [t(r_i) + v(r_i)] \equiv \sum_{i=1}^{A} h(r_i), \tag{2.7}$$

represents the mean-field Hamiltonian and

$$V_{RES} = V - \sum_{i=1}^{A} v(r_i) = \sum_{i,j=1;i<j}^{A} v(r_i, r_j) - \sum_{i=1}^{A} v(r_i), \tag{2.8}$$

represents the residual interaction.

Placing oneself in mean-field approximation, each nucleon can be considered as moving within an external field generated by the $A-1$ nucleons and, as mentioned above, in this way a strongly interacting fermionic system, can be considered equal a system of A non-interacting fermions in an external potential $v(r)$. The stationary states of a single particle bound to this potential can be calculated in analogy with the simple solution of a potential well problem in quantum mechanics.

The mean field Hamiltonian can be treated with simplicity considering the Schrödinger equation related to an A-nucleon system

$$H_{MF} \Psi_0(\vec{r}_1, \vec{r}_2, ..., \vec{r}_A) = E \Psi_0(\vec{r}_1, \vec{r}_2, ..., \vec{r}_A), \tag{2.9}$$

which can be factorized through the hypothesis that

$$\Psi_0(\overrightarrow{r}_1, \overrightarrow{r}_2, ..., \overrightarrow{r}_A) = \frac{1}{\sqrt{A!}} \sum_P (-1)^P \phi_{\alpha_1}(\overrightarrow{r}_1)\phi_{\alpha_2}(\overrightarrow{r}_2)...\phi_{\alpha_A}(\overrightarrow{r}_A), \tag{2.10}$$

where it is indicated with ϕ_{α_i} the single-particle function and the sum of P (which is the parity of the permutation) indicates all the possible permutations of the α_i. Replaced in the many-body Schrödinger equation (2.9) leads to a Schrödinger equation for a single nucleon

$$h(\overrightarrow{r})\phi_\alpha(\overrightarrow{r}) = \epsilon_\alpha \phi_\alpha(\overrightarrow{r}), \tag{2.11}$$

putting

$$h(\overrightarrow{r}) = t(\overrightarrow{r}) + v(\overrightarrow{r}) = \frac{-\hbar^2}{2m_N}\nabla^2 + v(\overrightarrow{r}). \tag{2.12}$$

Thus, one obtains that for a Schrödinger equation for many nucleons there is a solution determined as product of the single particle wave functions obtained by solving the Schrödinger equation for the single nucleon with respect to a given external potential.

The search for the average field $v(r_i)$ that best minimizes the residual interaction, as it happens in the atomic context, also in the nuclear case is obtained by means of a variational principle at the base of the best known method used for this purpose, the *Hartree-Fock method* (HF). In the nuclerar context, the most used method is the Hartree-Fock approximation, of which only a brief description is provided for its completeness. The HF theory aims to find the gound-state in the form (2.10) starting from H, without imposing a given mean-field. Then, among all the eigenfunctions describable by a Slater determinant, the ground state of the system under examination is calculated by minimizing the expected value of the energy

$$E = \langle \Psi_0 | H | \Psi_0 \rangle, \tag{2.13}$$

imposing the condition

$$\delta\left(\frac{\langle \Psi_0 | H | \Psi_0 \rangle}{\langle \Psi_0 | \Psi_0 \rangle}\right) = 0. \tag{2.14}$$

The orthonormality of the functions is guaranteed by adding a Lagrange multiplier to (2.14)

$$\delta[E - \sum_i \epsilon_{\alpha_i} \int d^3r \phi^*_{\alpha_i}(\overrightarrow{r})\phi_{\alpha_i}(\overrightarrow{r})]. \tag{2.15}$$

In carrying out the variation, it emerges that the multipliers used are nothing else that the single particle energies ϵ_α and we arrive at the following equation

$$\frac{-\hbar^2}{2m_N}\nabla^2\phi_\alpha(\overrightarrow{r}) + V_{HF}(\phi_i(\overrightarrow{r}))\phi_\alpha(\overrightarrow{r}) = \epsilon_\alpha\phi_\alpha(\overrightarrow{r}), \tag{2.16}$$

$$i = 1, 2, ..., A; \alpha = 1, 2, ..., \infty.$$

The equation thus obtained, has the form of the Schrödinger equation with less than the potential, which in this case is replaced with a functional relative to unknown wave functions. Given the non-linearity of (2.16), the solution is more complex than that of a classical Schrödinger equation. For this reason, the method provides an iterative and self-consistent process that leads to the solution of the equation (2.16). As a first step, we use a set of self test features $\psi^0_i(\overrightarrow{r})$ to calculate the initial potential term $V^0_{HF}(\overrightarrow{r})$, which will later be used to resolve (2.16) and get a new set of eigenfunctions $\psi^1_i(\overrightarrow{r})$ and eigenvalues ϵ^1_α. The latter are used to calculate a new potential term $V^1_{HF}(\overrightarrow{r})$ which, in turn, will generate an additional set of eigenfunctions and eigenvalues, and so on. The iterative process finds a conclusion only if the self-consistency is reached, i.e. the criterion is satisfied

$$||\phi^{n-1}_\alpha - \phi^n_\alpha|| < \text{limit condition} \tag{2.17}$$

Once the self-consistency is satisfied, the process will have generated a self-consistent mean-field $v_{HF}(\overrightarrow{r})$ with the eigenstate associates $\phi_\alpha(\overrightarrow{r})$ and eigenenergies ϵ_α.
The equation (2.13) can be applied separately considering the two constituent terms, kinetic and potential, obtaining respectively

$$\langle\Psi_0|T|\Psi_0\rangle = \sum_i -\frac{\hbar^2}{2m_i}\int d^3r\psi^*_i(\overrightarrow{r})\nabla^2\psi_i(\overrightarrow{r}), \tag{2.18}$$

$$\begin{aligned}\langle\Psi_0|V|\Psi_0\rangle &= \frac{1}{2}\sum_{i,j}\int\int d^3r d^3r' \psi_i^*(\overrightarrow{r})\psi_j^*(\overrightarrow{r}')v(\overrightarrow{r},\overrightarrow{r}')\psi_i(\overrightarrow{r})\psi_j(\overrightarrow{r}') \\ -\frac{1}{2}\sum_{i,j}\int\int d^3r d^3r' \psi_i^*(\overrightarrow{r})\psi_j^*(\overrightarrow{r}')v(\overrightarrow{r},\overrightarrow{r}')\psi_i(\overrightarrow{r}')\psi_j(\overrightarrow{r}) &= v_H + v_F\end{aligned} \tag{2.19}$$

Equation (2.19) is the sum of two contributions of which, the first is called *Hartree term* v_H or also *direct term*. It represents the overlap energy of the probability density of the system considered in the two bodies context. With

$$n(\overrightarrow{r}) = \sum_i \psi_i^*(\overrightarrow{r})\psi_i(\overrightarrow{r}). \tag{2.20}$$

The Hartree term can take a more compact form

$$v_H = \frac{1}{2}\int\int d^3r d^3r' n(\overrightarrow{r})v(\overrightarrow{r},\overrightarrow{r}')n(\overrightarrow{r}'). \tag{2.21}$$

The second term is the *exchange term* v_F or *Fock term*, whose presence is due to the fermionic nature of the particles studied. The Fock term is added accordingly to restore the antisymmetry and is not local due to the range of the interaction between two bodies, but it becomes so δ-force is used.
In the nuclear field, the nucleon-nucleon interaction causes the potential to be characterized by a short-range repulsive component, making the use of the Hartree-Fock equations problematic, since the direct term would diverge for $\overrightarrow{r} \approx \overrightarrow{r}'$. Therefore, the iterative procedure requires adequately parametrized potentials and forces, of which the best known are the forces of a Gaussian nature called *Gogny's forces* [3] and the *Skyrme forces* [2], which are zero-range forces and dependent by *Dirac's* δ.

2.0.3 Phenomenological potentials

To explain the regularities associated with the properties of the nuclei characterized by magic numbers and to considerably improve the liquid drop model, in the following years, the shell model, developed and used successfully in the atomic field, has also established itself in the nuclear context.
The shell model reproduces the energy levels through a closed shell structure respecting the Pauli principle, and the nuclear case differs from the atomic case due to a short range potential, *spin-spin* and *spin-orbit* interactions more relevant and there is no Coulomb potential of the nucleus, as the nucleons

produce and undergo the potential.

The simplest potential adopted is the **harmonic oscillator potential** in three dimensions

$$v_{HO}(r) = -V_0 + \frac{1}{2} m_N \omega^2 r^2. \tag{2.22}$$

Its simplicity has allowed an in-depth study that has led to the analytical knowledge of the main physical quantities associated with it. The related eigenfunctions, have the form

$$\Phi_{nlm_l}(r) = \frac{u_{n,l}}{r} Y_{lm_l}(\theta\psi). \tag{2.23}$$

The radial equation of Schrödinger thus rewritten

$$[\frac{-\hbar^2}{2m}\frac{d^2}{dr^2} + v(r) + \frac{l(l+1)}{r^2} - (\epsilon_{nl} + v_0)], \tag{2.24}$$

is resolved by imposing

$$u_{nl}(r) = N_{nl} q^{l+1} e^{-\frac{q^2}{2}} L_{n-1}^{l+\frac{1}{2}}(q^2), \tag{2.25}$$

$$L_p^a(z) = \frac{\Gamma(a+p+1)}{(p+1)} \frac{e^z}{z^a} \frac{d^p}{dz^p}(z^{a+p} e^{-z}), \tag{2.26}$$

$$N_{nl} = \frac{2(n-1)!}{b[\Gamma(n+l+\frac{1}{2}]^3}, \tag{2.27}$$

by set $b = \frac{r}{b}$, $b^2 = \frac{\hbar}{m\omega}$ and $L_p^a(z)$ are the Laguerre polynomials. The spectrum of energies for the harmonic oscillator can be constructed from its analytical form

$$\hbar\omega(2n + l + \frac{3}{2}) - v_0, \tag{2.28}$$

$$n = (n_r - 1). \tag{2.29}$$

The analytical form of the energy, shown above, shows a separation of the levels equal to $\hbar\omega$ and using the nuclear data for the radii to determine $\hbar\omega = 41/A^{\frac{1}{3}}\ MeV$ allows at the same time to reproduce the empirical shell gaps reasonably. Because of its conformation that diverges to infinity and does not goes to zero at great distances, the potential of the harmonic oscillator does not reproduce the correct behavior of long-distance eigenfunctions.

The **infinite square-well potential** represents a further simple form of single-particle potential, whose shape does not present the long-distance divergence problem highlighted in the harmonic oscillator potential. Also in this case, the analytical form of wave functions and energies is known. In fact, it is possible to write the eigenfunctions as

$$\Phi_{nlm_l}(r) = N_{nl} J_l(kr) Y_{lm_l}(\theta, \psi), \tag{2.30}$$

where N_{nl} is a normalization constant, $J_l(kr)$ are the functions of Bessel and $Y_{lm_l}(\theta, \psi)$ are the spherical harmonic functions. Such eigenfunctions must vanish for $r >= R$. The eigenvalues that define the energies referred to the eigenfunctions take the form

$$\epsilon_{nl} = \frac{\hbar^2 k_{nl}^2}{2m} - v_0. \tag{2.31}$$

Following this approach, the nearest shells can be obtained for total particle numbers of $2, 8, 18, 20, 34, 40, 58, ...$ but they do not represent the nuclear magic numbers.

The combination of the good features offered by these potentials can be obtained from the use of the **Woods-Saxon potential** defined as follows

$$v_{WS}(r) = \frac{-V_0}{1 + e^{\frac{r - R_N}{a_0}}}, \tag{2.32}$$

where $a_0 = 0.67 fm$ is the nuclear surface thickness, the nuclear radius is given by

$$R_N = r_0 A^{\frac{1}{3}} = 1.27 A^{\frac{1}{3}} fm, \tag{2.33}$$

and the term V_0 quantifies the depth of the potential well and is writable in the form

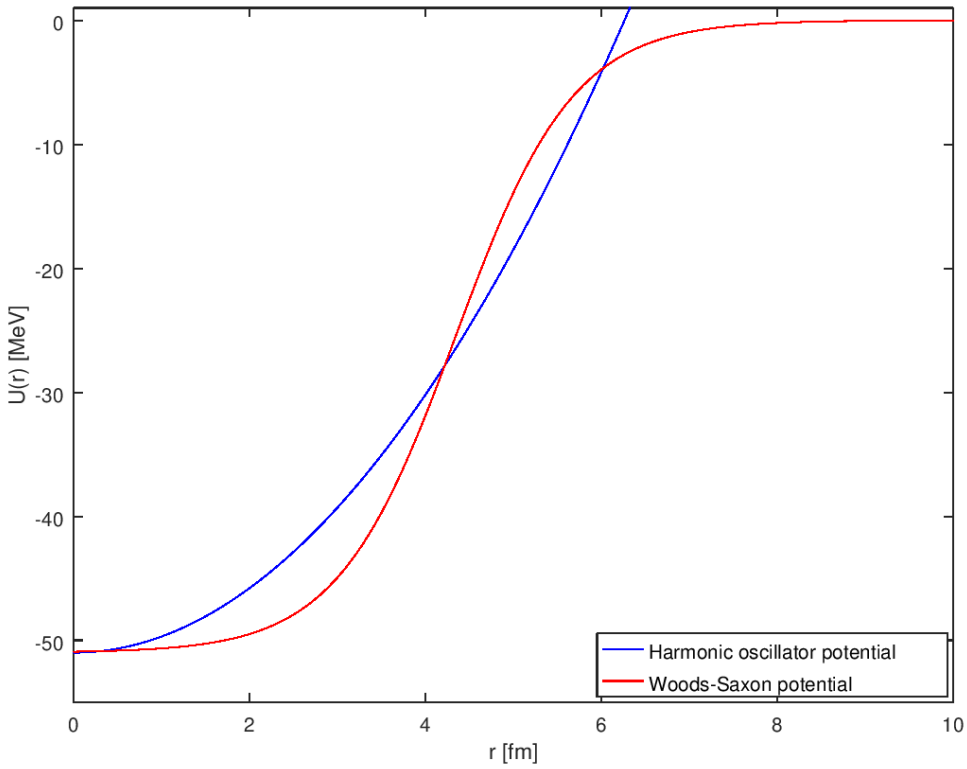

Figure 2.1: Comparison between the harmonic oscillator and Woods-Saxon potentials for the ^{40}Ca nucleus. The divergent trend of the harmonic oscillator potential is evident for large r.

$$V_0 = 51 \pm 33\frac{N-Z}{N+Z}\ MeV, \tag{2.34}$$

where the sign $(+)$ holds for the protons and the sign $(-)$ holds for the neutrons. The analytical form of the Woods-Saxon potential promotes the $p-n$ interaction with respect to the $p-p$ and $n-n$ interactions. As a consequence, an increase in the number of neutrons with respect to protons means that proton potential is deeper and the neutron potential is almost unchanged.

The Woods-Saxon potential alone does not reproduce the experimentally highlighted magic numbers that identify closed-shell nuclei, which can instead be riproduced if a spin-orbit term is added.

Spin-orbit interaction. The main effect of the spin-orbit term is to split in two the states characterized by the same value of the number of orbital angular momentum l, with an angular momentum of single particle defined as $j = l + \frac{1}{2}$ and $j = l - \frac{1}{2}$.

The nuclear spin-orbit interaction has significantly different origins from the atomic equivalent. The atomic spin-orbit interaction acts on the fine structure characterized by a scale of the order of millielectronvolt, therefore the resulting energy separation is of the order of a few electronvolt. It follows that

atypical shells are marginally affected by the action of the spin-orbit effect. On the contrary, for the nuclear case the spin-orbit splitting is of the order of millions of electronvolts. Instead, the eigenfunctions are not particularly affected by this effect. Moreover, the order of splitting in the nuclear context is inverse compared to the atomic one, this because the nuclear spin-orbit forces are not yet well understood. For the average field potential in the shell model, the spin-orbit term can take the form

$$v_{LS}(r) = v_{LS}^0(\frac{r_0}{\hbar})^2\frac{1}{r}[\frac{d}{dr}\frac{1}{1+e^{\frac{(r-R)}{a}}}]\overrightarrow{L}\cdot\overrightarrow{S}. \tag{2.35}$$

The dependence on r is phenomenological and its derivative produces a peak of the spin-orbit effect in the region of the nuclear surface. Taking advantage of the parameterization for Woods-Saxon (2.32), it is possible to define

$$v_{LS}^0 = 0.44V_0. \tag{2.36}$$

Coulomb interaction. In addition to the strong nuclear force, the protons also suffer from a repulsive force. Considering the nucleus as a sphere uniformly charged with radius R_n, having a charge density equal to

$$n_{chr}(r) = \frac{Zq_e}{\frac{4}{3}\pi R_n^3}, \tag{2.37}$$

the Coulomb term, then, can take the form

$$v_{coul.}(r) = \begin{cases} \frac{1}{2}\frac{Zq_e^2}{R_n}[3-(\frac{r}{R_n})^2] & r \leqslant R_n \\ \frac{Zq_e^2}{R_n} & r > R_n \end{cases} \tag{2.38}$$

A better rewriting of (2.38), allows to obtain a more realistic potential that resembles that associated with a Fermi distribution. at this purpose, [20] proposes the replacement of R_n with

$$R_U = R_n\sqrt{\frac{1+(5s^2/2R_n^2)}{1+(3s^2/4R_n^2)}}, \tag{2.39}$$

where is placed $s = 0.2fm$. This approximation does not include the term exchange and the direct term. To remedy to this lack, Slater in one of his articles [21] of 1951, proposes a further approximation starting

from the definition of local proton density valid as an exact result in infinite matter

$$E^{ex}_{coul.} = -\frac{3q_e^2}{4}(\frac{3}{\pi})^{\frac{1}{3}} \int d^3r n_p(r)^{\frac{4}{3}}, \tag{2.40}$$

with n_p proton density. Starting from (2.40), the Coulomb potential is obtained

$$V_{coul.}(r) = \frac{q_e^2}{2}[\int d^3r' \frac{n_p(r')}{|r-r'|} - (\frac{3}{\pi}n_p(r))^{\frac{1}{3}}], \tag{2.41}$$

in which the second term is identified as a term of exchange and the first term as a direct part, better defined as

$$V_{dir}(r) = q_e^2[\frac{1}{r}\int_0^r 4\pi n_p(r')r'^2 dr' + \int_0^\infty 4\pi n_p(r')r'^2 dr']. \tag{2.42}$$

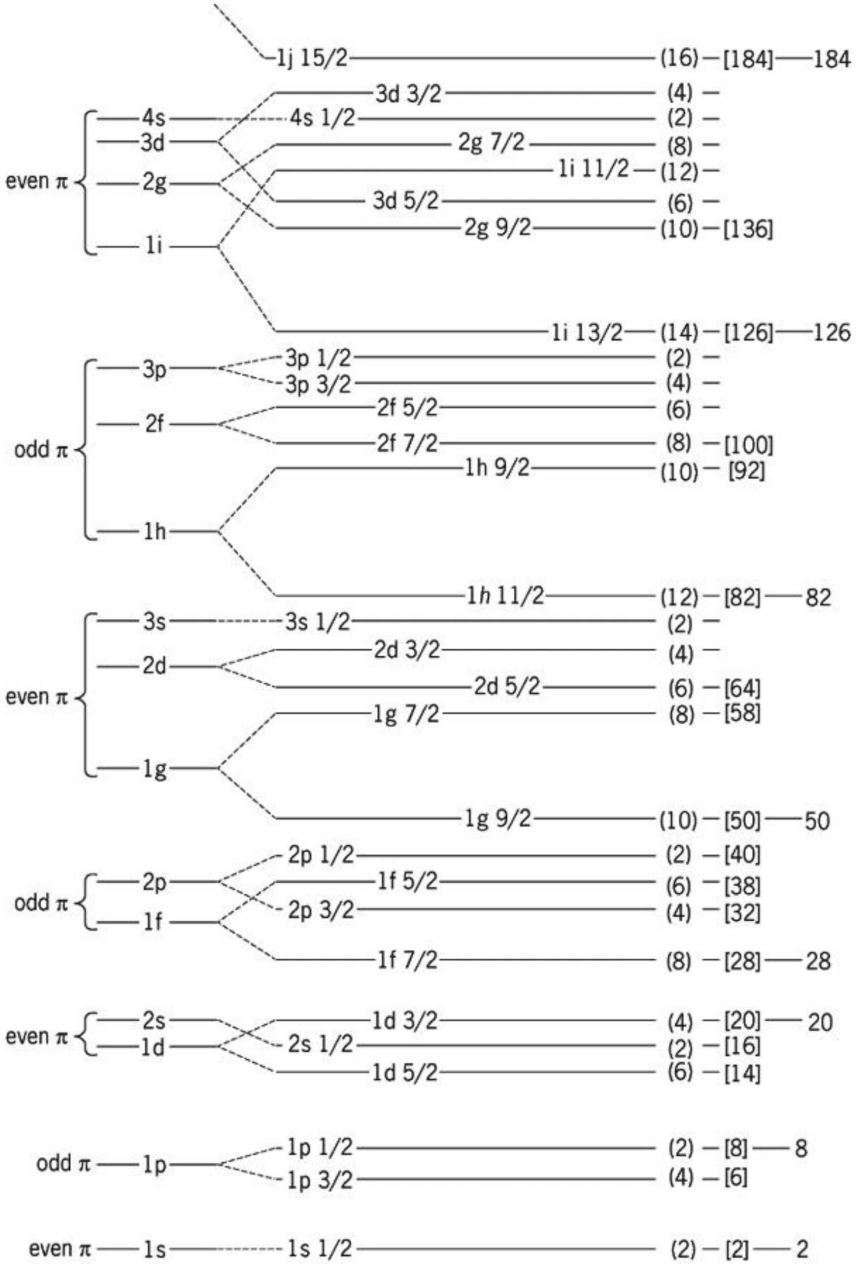

Figure 2.2: The nuclear shell structure.

Chapter 3

The Density Functional Theory

The Hartree-Fock method allows to obtain mean-field potentials starting from an interaction between nucleons. The single-particle wave function ψ_i can be written in terms of the Slater determinant and has a unique relationship with the HF densities. Then, it is possible to define the nucleon density as

$$n(r) = \sum_i |\psi_i(r)|^2 \tag{3.1}$$

The literature provides more than an alternative method to the classical HF to describe the nucleus, and in particular the consideration just mentioned, focuses on how advantageous it can be to introduce a density functional for the study of a nuclear system. The theory of Density Functional (DFT) is based on the idea of what has just been described, which represents a valid alternative to the HF method. This theory has origin and consolidation in the atomic field for the study of electron gas, but also in the molecular context it has found its place. It is quite natural to undertake this alternative way even in the nuclear case, considering that electrons and nucleons are both fermions. The present thesis work aims, in fact, to give a first approach of the use of inverse DFT in the description of a system of nucleons, albeit in an exploratory way, which is still missing in the literature. In the following, the theory will be presented both in its most general form and in a more practical formulation. Together, they will represent the mathematical setting on which to construct the nuclear model useful for achieving the pre-established purpose.

3.0.1 Hartree-Fock limitations in nuclear case

Before introducing the mathematical formalism of DFT, it is right to clarify why it is preferable, compared to the much more widely used HF theory. In this regard, G. Coló in his recent work [4], highlights the problems that can be encountered during the study of nuclear systems with HF. Following this, two cases will be presented in which the HF theory is unable to describe important nuclear properties such as saturation and effective mass.

In uniform SNM, the saturation point represents a minimum for particle energy (2.4) and its expansion leads to

$$e = e_0 + \frac{1}{2}K(\frac{n - n_0}{3n_0}) + \dots \tag{3.2}$$

K is called nuclear incompressibility and related to the rigidity of nuclear matter under compression and, indirectly, also to other observables.

In the case of asymmetric matter, the energy per particle depends on both the proton density n_p and the neutron density n_n. For simplicity, a change of variable is required

$$\beta = \frac{n_n - n_p}{n}, \tag{3.3}$$

and we get the expansion in β

$$e(n, \beta) = e(n, \beta = 0) + S(n)\beta^2. \tag{3.4}$$

This is the sum between the energy per particle in SNM (the first term) and the symmetry energy $S(n)$ required to change symmetric matter into neutron matter. The latter if expanded as a function of n lead to

$$S(n) = J + L(\frac{n - n_0}{3n_0}) + \frac{1}{2}K_{sym}(\frac{n - n_0}{3n_0})^2 + \dots \tag{3.5}$$

where J and L are two important parameters. The first is the value of the saturation density symmetry energy and from this the other parameters can be defined, like L (*slope parameter*), through first and second derivatives. the knowledge of these parameters plays an important role in the study of proton-neutron imbalance at different densities.

From the Fermi momentum (in SNM)

$$k_F = (\frac{3\pi^2 n}{2})^{\frac{1}{3}}, \tag{3.6}$$

and form the wave function in a uniform system

$$\phi_j = \frac{1}{\sqrt{\Omega}} e^{i \overrightarrow{k} \overrightarrow{r}}, \tag{3.7}$$

it is possible to derive from the (2.18) the expression for the kinetic part of the total energy in terms of density. The expression by particle takes the shape

$$t = \frac{T}{A} = \frac{2}{\pi^2} \frac{\hbar^2}{2m} \frac{k_F^5}{5} \frac{\Omega}{A} = \frac{2}{5} \frac{3\pi^2}{2} \frac{\hbar^2}{2m} n^{\frac{2}{3}}. \tag{3.8}$$

If we consider an interaction of range μ

$$V(\overrightarrow{r}_1, \overrightarrow{r}_2) = S e^{-\frac{\overrightarrow{r}_1 - \overrightarrow{r}_2}{\mu^2}}, \tag{3.9}$$

the direct and exchange terms of total energy per particle can be written as

$$\begin{aligned} v_H &= \frac{S}{2} \mu^3 \pi^{\frac{3}{2}} n \\ v_{xc} &= -\frac{S}{2} \frac{1}{\sqrt{\pi}} g(\mu k_F) \end{aligned} \tag{3.10}$$

where

$$g = \frac{2}{x^3} - \frac{3}{x} - (\frac{2}{x^3} - \frac{1}{x}) e^{-x^2} + \sqrt{x} erf(x). \tag{3.11}$$

The direct term goes with n, consistent with the short-range two-body interaction. The term of exchange, intrinsically dependent on density, has the opposite sign, highlighting an attractive force ($S < 0$). As a consequence, the kinetic contribution combined with the repulsion of the exchange term is too weak to allow saturation. Brink and Boeker, through their work [37], proposed to include exchange terms in the interaction. Considering the permutation of the particle 1 with the particle 2, it can be written

$$V(\overrightarrow{r}_1, \overrightarrow{r}_2) = S(1 - m + mP_M)e^{-\frac{|\overrightarrow{r}_1 - \overrightarrow{r}_2|^2}{\mu^2}}, \tag{3.12}$$

with P_M exchange operator, then the (3.10) can be rewritten as

$$\begin{aligned} v_H &= \frac{S}{8}(4 - 5m)\mu^3\pi^{\frac{3}{2}}n \\ v_{xc} &= \frac{S}{2}(5m - 1)\frac{1}{\sqrt{\pi}}g(\mu k_F). \end{aligned} \tag{3.13}$$

Now, the two terms v_H and v_{xc} are adequately weighted to achieve saturation with values of μ in the range $[0.5, 1.5]\ fm$. The HF scheme, however, are not sufficient to predict the empirical value of the parameters J and L.

Another issue using the HF method is the failure to reproduce the empirical value of the effective mass m^*/m. In fact, the definition of effective mass derives from the dispersion relation ϵ which binds the single-particle energy at its momentum. In a uniform system

$$\epsilon = \frac{\hbar^2 k^2}{2m} + \Sigma(k, \epsilon) \equiv \frac{\hbar^2 k^2}{2m^*}, \tag{3.14}$$

where Σ is the single-particle self-energy. From this, it is possible to obtain the effective mass

$$\frac{m^*}{m} = (1 + \frac{m}{\hbar^2 k}\frac{\partial\Sigma}{\partial k})(1 - \frac{\partial\Sigma}{\partial\epsilon})^{-1}. \tag{3.15}$$

If the Hartree-Fock equation (2.16) is conveniently rewritten with the exchange operator P_{12}

$$\langle j|-\frac{\hbar^2}{2m}\nabla^2|j\rangle + \sum_{l=1}^{N}\langle jl|V(1 - P_{12})|jl\rangle = \epsilon_j, \tag{3.16}$$

considering a flat wave function of the type (3.7), it can take the shape similar of the (3.14). Then, one can get

$$\Sigma_{\sigma,\tau}(k, \epsilon) = \sum_{\sigma',\tau'}\frac{\Omega}{(2\pi)^3}\int d^3k' \left\langle \overrightarrow{k}, \sigma, \tau; \overrightarrow{k}', \sigma', \tau' \middle| V(1 - P_{12}) \middle| \overrightarrow{k}, \sigma, \tau; \overrightarrow{k}', \sigma', \tau' \right\rangle. \tag{3.17}$$

Σ can be derived starting from the choice of V and give the value of the effective mass. However, into

the HF scheme, Σ does not depend on ϵ.

In a uniform system, the effective mass is clearly linked to the level density. In fact, higher its value, then shorter is the spacing. The same thing happens in the case of an non-uniform system, albeit less intuitively.

The considerations made so far show how an HF model fails to describe nuclei through the properties of bulk (such as saturation) or spectroscopic (such as effective mass) without the terms dependent on density in nuclear Hamiltonian. It is natural, therefore, to think that a theory based on the concept of density is better to describe the complex nuclear system.

3.0.2 The Hohenberg-Kohn theorems

Through the study of electronic systems, in 1964, P. Hohenberg and W. Kohn gave life to the Theory of Functional Density [5] in which the variational principle for ground state energy assumes the dependence on probability density in the presence of any external potential. Considering N interacting particles confined in a well-defined region and moving under the influence of an external potential $v(r)$, the Hamiltonian then assumes the form

$$\hat{H} = \hat{T} + \hat{V} + \hat{U} = -\sum_{i=1}^{A} \frac{\nabla^2}{2m_i} + \sum_{i=1}^{A} v_i(\overrightarrow{r}) + \sum_{i \neq j} u(\overrightarrow{r_i}, \overrightarrow{r_j}). \tag{3.18}$$

Assuming that the ground state is non-degenerate leads to its density being written in the following form

$$n(\overrightarrow{r}) := \langle \overrightarrow{r} | \Psi \rangle \langle \Psi | \overrightarrow{r} \rangle = \frac{1}{\sqrt{N}} \int d\overrightarrow{r}_1 ... d\overrightarrow{r}_A |\Psi(\overrightarrow{r}_1 ... \overrightarrow{r}_A)|^2, \tag{3.19}$$

where N is an the number of particles.

At this point, to prove that $v(\overrightarrow{r})$ is a unique functional of $n(\overrightarrow{r})$ unless an additive constant, we proceed by *reductio ad absurdum*. We assume that there is another potential $v'(\overrightarrow{r})$ relative to another ground state Ψ' and that gives rise to the same density $n(\overrightarrow{r})$. Now, Ψ and Ψ' can not be equal (unless $v'(\overrightarrow{r}) - v(\overrightarrow{r}) = const.$), as they satisfy two different Schrödinger equations. Indicating with H, E and H', E' the Hamiltonian and ground state energies associated respectively to Ψ and Ψ', for the ground state minimization property, we get

$$E' = \langle \Psi' | H' | \Psi' \rangle < \langle \Psi | H' | \Psi \rangle = \langle \Psi | H + V' - V | \Psi \rangle, \tag{3.20}$$

so that V is the potential energy associated with the external field, then

$$E' < E + \int d\overrightarrow{r}[v'(\overrightarrow{r}) - v(\overrightarrow{r})]n(\overrightarrow{r}). \tag{3.21}$$

By interchanging the quantities provided and without an index, we reach the same conclusion

$$E < E' + \int d\overrightarrow{r}[v(\overrightarrow{r}) - v'(\overrightarrow{r})]n(\overrightarrow{r}) \tag{3.22}$$

and adding (3.21) and (3.22), we reach the absurd

$$E + E' < E + E' \tag{3.23}$$

This shows that $v(\overrightarrow{r})$ is the only functional of $n(\overrightarrow{r})$ unless an additive constant. since H is determined from $v(\overrightarrow{r})$, then it is obvious that the whole ground state of the many-body system is a unique functional of the density $n(\overrightarrow{r})$.
It is therefore possible to formulate the first Kohn-Sham theorem

Theorem 1 - The Density as Basic Variable

> Given a system with A interacting fermions in an external potential v, there is a biunivocal correspondence between the total energy in the presence of v (defined as functional of the density n of the particles) and the density itself.

Since Ψ is a functional of $n(r)$, then also the kinetic and interaction energy are too. It is therefore convenient to define for each particle a universal functional valid for any external potential

$$F[n(\overrightarrow{r})] \equiv \langle \Psi | T + V | \Psi \rangle . \tag{3.24}$$

For a given potential $v(\overrightarrow{r})$, the functional energy is writable in the form

$$E_v[n] \equiv \int v(\overrightarrow{r})n(\overrightarrow{r})d\overrightarrow{r} + F[n], \tag{3.25}$$

obviously, for the correct $n(\overrightarrow{r})$, the functional $E_v[n]$ equals the value of the E energy of the ground-state. For all the densities that satisfy the condition

$$\int drn(\overrightarrow{r}) = N, \tag{3.26}$$

it is possible to show that $E[n]$ assumes its minimum value for a precise density $n(\overrightarrow{r})$.
Maintaining the constant particle number, the functional energy of the Ψ' state

$$\mathcal{E}_v[\Psi'] = \left\langle \Psi' \middle| V \middle| \Psi' \right\rangle + \left\langle \Psi' \middle| T + U \middle| \Psi' \right\rangle, \tag{3.27}$$

has its minimum in the correct ground-state Ψ obtained from arbitrary changes of Ψ'.
If one maps Ψ' as the ground-state associated with a different external potential $v'(\overrightarrow{r})$, then by means of the (3.27) and (3.24), one gets

$$\mathcal{E}_v[\Psi] = \int v(\overrightarrow{r})n(\overrightarrow{r})d\overrightarrow{r} + F[n] < \int v(\overrightarrow{r})n'(r)d\overrightarrow{r} + F[n'] = \mathcal{E}_v[\Psi'], \tag{3.28}$$

in this way it is shown that the minimization property of (3.25) can be established in relation to all the functional densities $n'(r)$ associated by as many external potentials $v'(r)$. It is then possible to enunciate the second DFT theorem

Theorem 2 - The Variational Principle

The functional energy $\mathcal{E}[n]$ has a minimum at the exact density of the ground-state and at this point assumes exactly the value of the energy of the ground-state of the system.

3.0.3 The Kohn-Sham equations

In the months following the work presented with his colleague Hohenberg, Walter Kohn together with Lu Jeu Sham exploited the formalism introduced with the DFT to arrive at a concrete application of the theory itself.
As reported in a further publication [6], a step forward is to consider a non-homogeneous system of interacting fermions subject to an external potential and approximate it. If it is approximated by a system of non interacting fermions, with the imposition that the density $n(r)$ remains unchanged. Then

it will be possible to attribute to each particle an eigenfunction ψ_i that takes the name *Kohn-Sham orbital*. The advantage staying within this approximation, is that one has a total wave function corresponding to a Slater determinant, but even more useful is the possibility of having an associated density associated with it writable as sums of the single eigenfunctions

$$n(\overrightarrow{r}) = \sum_i |\psi_i|^2. \tag{3.29}$$

Explicitating the contributions to the functional density $F[n(r)]$ defined in (3.24), we obtain

$$F[n(\overrightarrow{r})] = T_S[n] + E_{int}[n], \tag{3.30}$$

where $T_s[n]$ represents the kinetic energy of the non-interacting system with density $n(\overrightarrow{r})$ and $E_{int}[n]$ is the interaction energy which, as already defined for the (2.19), consists of a direct term (of Hartree) E_H and an exchange term and correlation E_{xc} representing the residual interaction energy. Then, the total energy of the system is writable as

$$E[n] = T_s[n] + E_{int}[n] + \int dr v_{ext}(\overrightarrow{r}) n(\overrightarrow{r}), \tag{3.31}$$

if

$$T_s[n] = \sum_i -\frac{1}{2} \int d\overrightarrow{r} \psi_i^*(\overrightarrow{r}) \triangle \psi_i(\overrightarrow{r}). \tag{3.32}$$

As previously done for Hartree-Fock with the equations (2.13) and (2.15), in the same way we proceed in this case in search of the functional minimum, imposing

$$\delta E = 0. \tag{3.33}$$

Moreover, the approximation of non-iteracting fermions imposes the orthogonalization of the wave functions by means of a Lagrange multiplier added to (3.33)

$$\delta(E - \sum_i \epsilon_i \int d\overrightarrow{r} \psi_i^*(\overrightarrow{r}) \psi_i(\overrightarrow{r}) = 0, \tag{3.34}$$

and the condition of conservation of the number of fermions [1]

$$\int \delta n(\overrightarrow{r}) d\overrightarrow{r} = 0. \tag{3.35}$$

By carrying out the variation with respect to ψ_i*, explicitating the (3.34) in its components, we arrive at the following expression

$$\begin{aligned} \frac{\delta}{\delta \psi_i^*}(\sum_i -\frac{1}{2}\int d\overrightarrow{r}\psi_i^*(\overrightarrow{r})\triangle\psi_i(\overrightarrow{r}) + E_{xc}[n(\overrightarrow{r})] + \\ + \int v_{ext}(\overrightarrow{r})n(\overrightarrow{r})d\overrightarrow{r} - \sum_i \epsilon_i \int \psi_i^*(\overrightarrow{r})\psi_i(\overrightarrow{r})d\overrightarrow{r}) = 0, \end{aligned} \tag{3.36}$$

and considering that

$$\begin{aligned} \frac{\delta n}{\delta \psi_i^*} &= \psi_i \\ \frac{\delta n}{\delta \psi_i^*} &= \frac{\delta n}{\delta \psi_i^*}\frac{\delta}{\delta n} = \psi_i \frac{\delta}{\delta n}, \end{aligned} \tag{3.37}$$

then one comes to write the *Kohn-Sham equation*

$$[-\frac{\triangle}{2} + \frac{\delta E_{xc}[n(\overrightarrow{r})]}{\delta n(\overrightarrow{r})} + v_{ext}(\overrightarrow{r})]\psi_i(\overrightarrow{r}) = \epsilon_i \psi_i(\overrightarrow{r}), \tag{3.38}$$

which can be written by defining

$$\frac{\delta E_{xc}[n(\overrightarrow{r})]}{\delta n(\overrightarrow{r})} + v_{ext}(\overrightarrow{r}) = v_{KS}(\overrightarrow{r}) \tag{3.39}$$

which gives the (3.39) an appearance similar to a Schrödinger equation

$$[-\frac{\triangle}{2} + v_{KS}(\overrightarrow{r})]\psi_i(\overrightarrow{r}) = \epsilon_i \psi_i(\overrightarrow{r}) \tag{3.40}$$

This last writing of the Kohn-Sham equation brings to evidence the term $v_{KS}(\overrightarrow{r})$ which refers to an effective potential associated with the fermionic system considered up to now. It is therefore evident that

[1] The (3.35) represents the normalization condition.

the initial system of interacting particles can be described more simply in terms of DFT. The independent particle approximation makes it possible to define a Kohn-Sham orbital represented by an eigenfunction for each single particle, whose motion is independent from that of the other particles, and takes place under the influence of a common potential and here reproduced by $v_{KS}(\overrightarrow{r})$. The latter, turns out to be the unique functional of the density $n(\overrightarrow{r})$ described by the first theorem of Hohenberg and Kohn. Thus, if the density $n(\overrightarrow{r})$ is known, it is always possible to deduce its effective potential.

Chapter 4

Inverse Kohn-Sham Problem

The success of the density functional theory (DFT) is largely due to the introduction of exchange and correlation functions used as input for the DFT's *direct problem* solution, ie to solve the Kohn-Sham equation and obtaining a fermion density relative to the ground state of any considered, finite or periodic system. The *inverse problem*, consists in extracting the potential representative of the system under investigation by starting from the fermionic densities.

Both problems share the same Kohn-Sham equations to be solved, but they differ for the solutions. The inverse problems are commonly studied because they mathematically describe the structure of matter in scattering experiments. In the following chapter, all the elements useful for the development of the model will be presented, highlighting the criticalities encountered during the implementation phase and the conditions necessary to obtain accurate results.

From a practical point of view, it was decided to implement the code from scratch, although the choice of solvers for the Schrödinger equation already developed is wide. This choice is justified by obtaining a compact solution of the project by developing a mathematical model with the cleanest architecture possible to bequeathed. To this end, it was decided to make use of the C ++ programming language in its most modern version (C++14, C++17). Through the great modularity of object-oriented programming, it was possible to write easily accessible, correctable and reusable code in other projects. Furthermore, a programming made in this way simplifies the work of expanding the project.

At the end of the chapter, the block diagram of the entire model is shown in the figure (4.2). Starting from an initial potential, through the Schrödinger solver the Kohn-Sham equation is solved and then the theoretical density is calculated. Then, a potential is produced from the inverse Kohn-Sham equations that if it does not satisfy the convergence condition, it will itself become the starting potential for a new

elaboration. In this way we start of an iterative process that will end only if the convergence condition is satisfied.

4.0.1 Direct problem

The solution of the direct problem represents the first step to be taken to develop the mathematical model under discussion. As already described, the Kohm-Sham equations have the same form of a Schrödinger equation of which, being an ordinary differential equation of the second order, the resolutive method is well known. Considering non-deformed systems but having a spherical symmetry, it is possible to write the total wave function as a factorization of three terms dependent on the three spherical coordinates

$$\Psi(r,\theta,\phi) = R(r)\Theta(\theta)\Phi(\phi) \tag{4.1}$$

Of the three components, the one of interest for the development of the model is the only radial component. Therefore, let us $u(r) = rR(r)$ and Kohn-Sham equation takes the form

$$[-\frac{\hbar^2}{2m}\nabla_r^2 + \frac{l(l+1)\hbar}{2mr^2} + V_{KS}(r)]u(r) = Eu(r), \tag{4.2}$$

with

$$\nabla_r^2 = \frac{1}{r^2}\frac{d}{dr}(r^2\frac{d}{dr}). \tag{4.3}$$

The equation is solved by imposing boundary conditions equal to

$$\begin{gathered}\lim_{r\to 0} u(r) \propto r^{l+1} \\ \lim_{r\to 0} u'(r) \propto (l+1)r^l.\end{gathered} \tag{4.4}$$

The solution of (4.2) implies the knowledge of the eigenvalues, a further unknown of the direct problem. It is possible to determine them considering that the nuclear potential can be approximated to a potential well, outside of which, the eigenfunctions of the problem must be considered exponentially suppressed to 0. This additional boundary condition imposed on the problem's eigenfunctions allows a value of the energy eigenvalue to be considered correct if, when the (4.2) is resolved, the relative eigenfunction tends

to zero beyond the nuclear radius. If the equation is integrated up to a given maximum radius, then a value E of energy can be considered an eigenvalue of the problem if it satisfies the condition

$$|u(r_{max})| < \epsilon, \tag{4.5}$$

with $\epsilon \sim 10^{-8}$.

shooting method - In the model under development, it was decided to identify the eigenvalues of the problem by means of the *shooting method*. This is best known for solving regular (non-eigenvalue) problems at two-point boundary values, but it can also be successfully used to solve eigenvalue problems as in the case of Kohn-Sham's direct problem. Below is a schematic explanation of how the shooting method works

- Starts from a range of possible arbitrarily large eigenvalues, whose extremes are given by E_1 and E_2, respectively the higher and lower eigenvalues.
- Solves the Kohn-Sham equation for the eigenvalue E_2 and calculates the relative eigenfunction.
- The newly constructed eigenfunction nodes are counted in the range of radius $[0, r_{max}]$. These must be equal to the total quantum number n that characterizes the state under examination. If the number of nodes exceeds the value of n, the interval is shrunk by decreasing E_2. If the number of nodes is less than the value of n, then the interval is widened by increasing E_2. The process stops when, recalculating the eigenfunction every time, we get that the number of nodes equals n.
- We proceed to evaluate the sign of the function in r_{max}.
- We calculate a first intermediate eigenvalue, by means of a first bisection of the interval, defining the value $E_t = (E_1 + E_2)/2$ and calculating the relative eigenfunction.
- Reassigns the value of E_t to E_1 or E_2 if the sign of the eigenfunction evaluated in r_{max} is negative or positive respectively. The importance of evaluating the sign in r_{max} lies in the fact that in the bisection one evaluates $\psi(E_t, r_{max})$, but only E_t varies and r_{max} remains fixed. The algorithm that counts the nodes of the eigenfunction, always returns a wider range than necessary. If for n nodes the eigenfunction must necessarily tend to 0 in r_{max}, this condition must also be maintained during the bisection. If one changes the sign to r_{max} it means one has no more n nodes, but have $n - 1$.
- Then, one starts a process of bisection in which the value of E_t is reassigned to E_1 or E_2, with the

same procedures described in the previous point, which aims to narrow down more and more the interval around the desired eigenvalue. The process finds its termination when the condition is met

$$|E_2 - E_1| < \epsilon \tag{4.6}$$

- At the end of the bisection, the eigenvalue sought will be given by E_1

Its important to note that there is no restriction on the initial guess eigenvalues, as the algorithm should always converge. However, special care must be taken as to how the range of possible eigenvalues consistent with a given number of eigenfunction nodes is determined. Indeed, a common approach in the literature [30] suggests to expand or shrink the range of possible energies by fixed multiplicative factors, respectively larger and smaller than 1. An obvious shortcoming of this choice is that, in case both of our initial guess eigenvalues have the wrong sign, the algorithm will fail to converge around zero. A more robust choice is to adjust the interval of energies by adding or substracting an arbitrarily small epsilon after each iteration.

The calculated eigenfunctions must be normalized and, in spherical symmetry, this condition is expressed as

$$\int_0^\infty |u(r)|^2 dr = 1. \tag{4.7}$$

The eigenfunctions thus normalized must satisfy a further condition of normalization to the number of particles

$$\int n(r)dr = \sum_\alpha (2j_\alpha + 1) + \int u_\alpha^2(r)dr = \sum_\alpha (2j_\alpha + 1), \tag{4.8}$$

where with α we mean the set of quantum numbers $n_\alpha, l_\alpha, j_\alpha$ and $(2j_\alpha + 1)$ represents the orbital occupation number.

In the implementation of this model part, the equation (4.2) is resolved by using the *Runge-Kutta* method in the fourth order and with an integration step of $h = 0.1fm$.

From the eigenfunctions of the single nucleons thus obtained it is possible to determine their density [1] as

[1] If spin-orbit interaction is not taken into account, (4.9) takes the form $n(r) = \frac{1}{4\pi r^2} \sum_\alpha 2(2l_\alpha + 1)u_\alpha^2(r)$ with $\alpha = n_\alpha, l_\alpha$ and $2(2l_\alpha + 1)$ is the occupation number.

Table 4.1: Comparison between the eigenvalues obtained by the shooting and theoretical eigenvalues for the harmonic oscillator potential.

n	n_r	l	$E_{theo.}$	$E_{shooting}$
0	1	0	15	15.0000
1	1	1	25	24.9996
2	1	2	35	35.0000
2	2	0	35	35.0001

$$n(r) = \frac{1}{4\pi r^2} \sum_{\alpha} (2j_\alpha + 1) u_\alpha^2(r). \tag{4.9}$$

The calculation of the theoretical density (4.9), also a solution to the direct problem, takes place by means of the sum of the single nucleon eigenfunctions for the number of occupations of the involved orbitals. To arrive at the solutions of the problem, the quantum numbers that define the involved orbitals already ordered according to the shell model are directly passed to the solver of the Kohn-Sham equation. This approach may seem "*rigid*", and indeed it is, but in the following context it can be used without particular problems. This allows you to avoid unintentional exchanges of levels very close to each other by the shooting of the eigenvalues and allows a reduction in execution times, especially for the simulation of heavy nuclei.

First test - To test the goodness of the code so far written, a practical test was used. The Kohn-Sham equation is in effect a Schrödinger equation. Taking advantage of this similarity, it was possible to test the correct operation of the solver, in particular the parts related to the Runge-Kutta and the shooting. The potential of the harmonic oscillator as defined by (2.22), whose energies assume the analytical form (2.28), has been used as effective potential. Considering a system composed of 20 neutrons, the figure 4.1, shows the relative eigenfunctions that are comparable with what is reported in the literature. The table 4.1, on the other hand, shows the good accuracy of the eigenvalues calculated by the model compared to the exact ones.

4.0.2 Inverse problem

Before describing the inversion method used in the model, it is useful to provide a general overview of the main differences between the direct problem and the inverse problem, highlighting the limitations and problems that could be encountered.

In the case of the inverse problem, the Kohn-Sham equations are the same ones involved in the direct

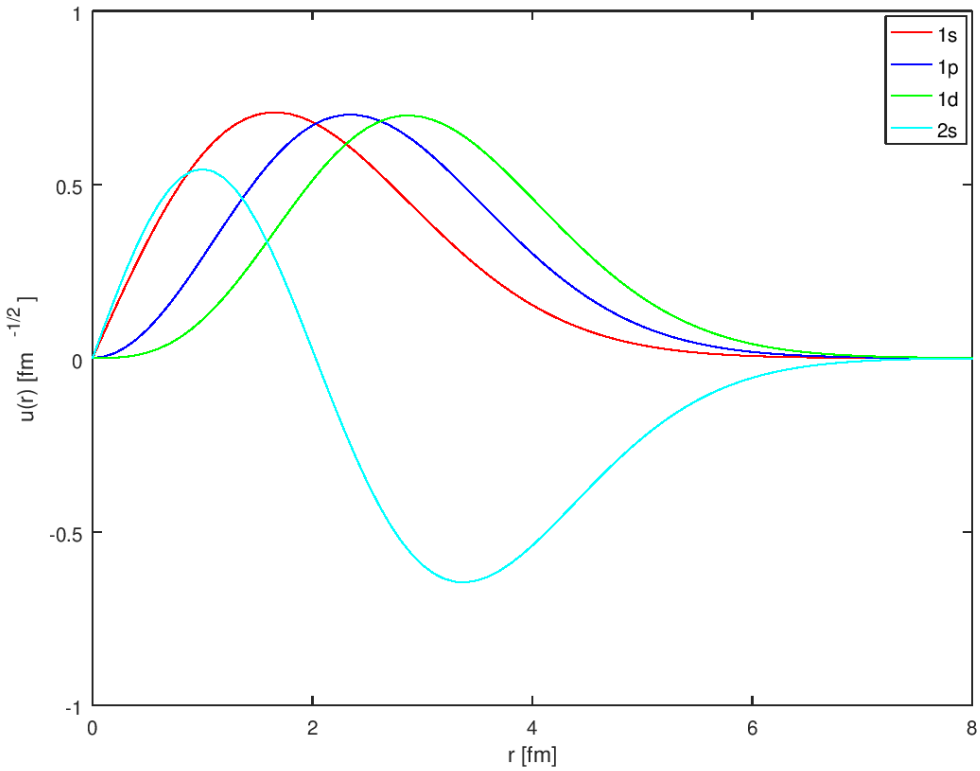

Figure 4.1: Eigenfunctions of the harmonic oscillator related to the first 4 nuclear orbitals obtained with $\hbar\omega = 10MeV$ and step $h = 0.001$.

problem, they differ only for the solutions. The inverse problem of Kohn-Sham presents the following equations

$$\epsilon_j \underline{\phi_j(\overrightarrow{r})} = [-\frac{\triangle}{2} + v_{KS}([n], \overrightarrow{r})]\underline{\phi_j(\overrightarrow{r})}, \tag{4.10}$$

$$n(\overrightarrow{r}) = 2\sum_{j=1}^{N} |\underline{\phi_j(\overrightarrow{r})}|^2, \tag{4.11}$$

$$v_{KS} = v_{ext}(\overrightarrow{r}) + v_H([n], \overrightarrow{r}) + \underline{v_{xc}([n], \overrightarrow{r})}, \tag{4.12}$$

in which the unknowns of the problem are underlined. A comparison between these equations and those used for solving the direct problem, leads to consider how the equation (4.2) is a non-linear eigenvalue equation due to the density dependence that the Kohn-Sham potential possesses, while the (4.10) is a linear eigenvalue equation. Despite this, the inverse problem turns out not be linear due to the nonlinearity due from (4.11). This non-linearity present in both cases, leads to a great sensitivity from the initial data. The type of initial data used is particularly important and if this is lacking or too far from the expected result, the achievement of convergence is not guaranteed by many inversion methods. A further difference between the direct and the inverse problem lies in the fact that in the latter there is no certain knowledge of the boundary conditions in many cases. The density constraint can univocally determine the behavior of the orbitals at the boundaries. If boundary conditions are imposed, then it is important that these are agree with density constraints.
In general, a well-posed problem should have the following three properties

- **Existence**: there must be a solution to the problem;
- **Uniqueness**: there must be at least one solution to the problem;
- **Stability**: the solution depends continuously on the data.

Mathematically, the existence of a solution can be strengthened by enlarging the solution space. If a problem has more than one solution, the model is missing information that needs to be added. Finally, if a problem lacks stability, then it will be impossible to reach a solution. Without continuous data dependence, any attempt to find the solution would lead to errors, or the solution obtained would have nothing to do with the real solution. A problem that does not reflect these properties is called *ill-posed*.

From this point of view, in DFT the uniqueness of the solution is satisfied by the density in both cases, direct and inverse, but it is not for the resulting Kohn-Sham orbitals. In fact, from the (4.11) for the inverse problem (but the same also applies to the direct problem) we can see how the density depends on the squared absolute value of the KS orbital. Therefore each KS orbital can be unique at most for one phase factor and each of their unitary transformation will produce the same density. Also the potential KS, which in the inverse problem is defined by (4.12), is a source of non-uniqueness. It can be considered as such at most for a constant. A density-to-potential inversion method will therefore have to provide for adequate restrictions to put the problem as well-posed.

Inversion algorithm - For the development of this model, we have considered the inversion algorithm proposed by *van Leeuwen* and *Baerends* proposed in their work [7] dated 1993 which provides an iterative method for solving the inverse problem of Kohn-Sham.
Taking the equation (4.10), we multiply both members by ϕ_j^* and adding on the index j we get

$$\sum_{j=1}^{N} \epsilon_j |\phi_j(\overrightarrow{r})|^2 = \sum_{j=1}^{N} -\phi_j^*(\overrightarrow{r}) \frac{\triangle}{2} \phi_j(\overrightarrow{r}) + v_{KS}([n], \overrightarrow{r}) |\phi_j|^2. \tag{4.13}$$

Dividing by $n(r)$ and isolating the potential, we get

$$v(r) = \frac{1}{n(\overrightarrow{r})} \sum_{j=1}^{N} -\phi_j^*(\overrightarrow{r}) \frac{\triangle}{2} \phi_j(\overrightarrow{r}) + v_{KS}([n], \overrightarrow{r}) |\phi_j|^2. \tag{4.14}$$

At this point, it is possible to define an iterative process that exploits this equation. By changing the density to the denominator with a target density $\widetilde{n}(\overrightarrow{r})$, which may have experimental or theoretical simulations, the (4.14) takes the form

$$v^{k+1}(\overrightarrow{r}) = \frac{1}{\widetilde{n}(\overrightarrow{r})} \sum_{j=1}^{N} -\phi_j^{k*}(\overrightarrow{r}) \frac{\triangle}{2} \phi_j^k(\overrightarrow{r}) + v_{KS}^k([n], \overrightarrow{r}) |\phi_j^k|^2 = \frac{n(\overrightarrow{r})^k}{\widetilde{n}(\overrightarrow{r})} v(\overrightarrow{r})^k, \tag{4.15}$$

where k expresses the iteration index. The equation shows how the restriction on the potential output at each iteration acts. In regions where one has $n(\overrightarrow{r})^k > \widetilde{n}(\overrightarrow{r})$, the potential $v(\overrightarrow{r})^{k+1}$ increases, instead in the regions where one has $n(\overrightarrow{r})^k < \widetilde{n}(\overrightarrow{r})$, the potential $v(\overrightarrow{r})^{k+1}$ decreases.
The whole iterative process must converge to a potential that is a solution to the inverse problem. The iteration is then stopped when the convergence condition is met

$$\frac{max_r|n^k(\overrightarrow{r}) - \widetilde{n}(\overrightarrow{r})|}{\widetilde{n}(\overrightarrow{r})} < \epsilon, \tag{4.16}$$

with ϵ equal to 1% of the target density $\widetilde{n}(r)$. To avoid large potential oscillations during iteration, a prefactor is required that imposes the condition

$$1 - \delta < \gamma \frac{n^k(\overrightarrow{r})}{\widetilde{n}(\overrightarrow{r})} < 1 + \delta, \tag{4.17}$$

where $\delta \approx 0.05$ and γ is the prefactor, which must be chosen to better modulate the output potential. A wide value of the prefactor generates large oscillations of potential putting convergence at risk, while a low value leads to small changes in potential that leads to longer simulation times.

Adaptation to the nuclear case - As repeatedly repeated, the whole discussion built on the concepts of DFT and Kohn-Sham equations is devoted to the study of electronic systems. Also the vLB method is not far behind and for this reason it is important to make some clarifications.
The vLB method increases the potential to reduce the theoretical density if it is higher than the target density. This correction finds application in case the potential is positive, but in the nuclear case it is not valid. In fact, in mean field approximation, a nuclear potential has an attractive nature and is comparable to a potential depth that tends to a finite value inside the nucleus. The final result that would be used, for the study of a nuclear system, the algorithm as it was developed would lead to results contrary to what is expected. It is clear that it is necessary to make changes to better adapt the iterative method to the case under study. Defined

$$\delta = \frac{n^k(\overrightarrow{r})}{\widetilde{n}(\overrightarrow{r})} - 1, \tag{4.18}$$

then the (4.15) becomes

$$v^{k+1}(\overrightarrow{r}) = \frac{n(\overrightarrow{r})^k}{\widetilde{n}(\overrightarrow{r})} v^k(\overrightarrow{r}) = (1 + \delta) v^k(\overrightarrow{r}). \tag{4.19}$$

In the nuclear case, one would like the potential to meet the conditions as schematized

$$
\begin{aligned}
n^k(\overrightarrow{r}) > \widetilde{n}(\overrightarrow{r}) &\Rightarrow v^{k+1}(\overrightarrow{r}) < v^k(\overrightarrow{r}),\\
n^k(\overrightarrow{r}) = \widetilde{n}(\overrightarrow{r}) &\Rightarrow v^{k+1}(\overrightarrow{r}) = v^k(\overrightarrow{r}),\\
n^k(\overrightarrow{r}) < \widetilde{n}(\overrightarrow{r}) &\Rightarrow v^{k+1}(\overrightarrow{r}) > v^k(\overrightarrow{r}).
\end{aligned}
\tag{4.20}
$$

In relation to δ, these conditions would be met if the equation (4.19) was written as

$$
v^{k+1}(\overrightarrow{r}) = (1-\delta)v^k(\overrightarrow{r}). \tag{4.21}
$$

Substituting the definition of δ in the latter, we obtain a new inversion algorithm, appropriately adapted to the nuclear case and rewritten in terms of density

$$
v^{k+1}(\overrightarrow{r}) = [2 - \frac{n(\overrightarrow{r})^k}{\widetilde{n}(\overrightarrow{r})}]v^k(\overrightarrow{r}). \tag{4.22}
$$

In this way, the algorithm increases by a factor δ the depth of the potential in those regions where it occurs that the theoretical density is smaller than the target density, attracting the eigenfunctions in those regions and decreases the depth by a factor of δ.

The presence of the Coulomb interaction in the study of protons leads to positive parts in the potential. In this case, the algorithm in its original definition remains valid (4.15).

Therefore, in the nuclear case, the inversion algorithm envisaged in the VLB method is summarized as follows

$$
v^{k+1} = \begin{cases} [2 - \frac{n(\overrightarrow{r})^k}{\widetilde{n}(\overrightarrow{r})}]v^k(\overrightarrow{r}) & v^k(\overrightarrow{r}) < 0 \\ \frac{n(\overrightarrow{r})^k}{\widetilde{n}(\overrightarrow{r})}v^k(\overrightarrow{r}) & v^k(\overrightarrow{r}) > 0 \end{cases} \tag{4.23}
$$

To avoid large potential fluctuations at each step during the iteration process, the condition (4.17) can be rewritten as

$$
1 - \delta < \gamma[2 - \frac{n^k(\overrightarrow{r})}{\widetilde{n}(\overrightarrow{r})}] < 1 + \delta, \tag{4.24}
$$

where one has $\delta \approx 0.05$ and γ is the prefactor.

The initial potential - The iterative process described so far, returns a potential at each step starting from the potential of the previous step. Obviously, in order to start the iterative process, it is necessary to provide an initial potential to allow the first step to take place. As already discussed above, the solving methods of the inverse problems are particularly sensitive to the initial inputs. The same authors of the vLB method, as well as the authors of [8], recommend the use of an initial potential that does not deviate too much from what is expected. In the present work, it was thought to consider as initial potential the Woods-Saxon potential (2.32) in its canonical parametrization as reported in the literature. This potential, even today, is among the most appreciated and studied in medium field approximation. In the simulation of proton cases, the presence of the repulsive interaction term is required and, therefore, the Coulomb term defined as the (2.38) is added to the initial potential. The presence of the spin-orbit interaction (2.35) is necessary to reproduce the phenomenology of experimental evidence. Then a further term is added to the initial potential which, for convenience, is rewritten as

$$v_{LS}(r) = \frac{k_0}{r}(\frac{r_0}{\hbar})^2 \frac{1}{r}[\frac{d}{dr}\frac{1}{1+e^{\frac{(r-R)}{a}}}]\overrightarrow{L}\cdot\overrightarrow{S}, \tag{4.25}$$

where

$$\overrightarrow{L}\cdot\overrightarrow{S} = \frac{\hbar^2}{2}[j(j+1) - l(l+1) - \frac{3}{4}]. \tag{4.26}$$

In general, then, the initial potential can be defined as

$$v(r) = v_{WS}(r) + v_C(r) + v_{LS}(r). \tag{4.27}$$

During the development and use of the model, other initial potentials of different nature were also examined. For more details, refer to the Results chapter, where their use is explained with greater attention to the context under study.

4.0.3 Empirical densities

The inversion algorithm in the vLB method is suitable for the use of target densities that can be of different nature. It is possible to use densities coming from Monte Carlo or Hartree-Fock simulations, or densities coming from experimental investigations.
In the present work, we refer mainly to density of experimental origin, whose nature is described below.

Experimental Densities - The experimental densities that are most available come from electronic scattering experiments and minimally from hadron scattering. A good collection of data from electronic scattering experiments can be found in a *De Vries* [9] publication where data were reported for several well-parameterized nuclei.

The use of this kind of experimentation to study the nuclear structure is particularly appreciated because of an already deep knowledge of the electron-nucleus interaction. Being of low intensity, the presence of multiple scattering in an experiment leads to negligible effects at the first order. Furthermore, the scattering process is described by the perturbation theory.

In detail, during the experiment, an electron beam is directed towards nuclear target. These, by means of their Coulomb field, deviate with a certain angle the trajectory of the electrons. Precisely from the measurement for different angles of the cross sections it is possible to trace the charge density of the examined nuclei.

Within in *Plane Wave Born Approximation* (PWBA), the relationship implicitly linking the charge density with the cross section is given by

$$\frac{d\sigma(q)}{d\Omega} = \sigma_M f_{rc} |F(q)|^2, \tag{4.28}$$

where σ_M is the cross section of Mott, q the transferred momentum and $F(q)$ is the form factor and f_{rc} is the recoil term

$$f_{rc} = (1 + \frac{2\epsilon}{M_A} sin^2 \frac{\Theta}{2})^{-1}, \tag{4.29}$$

where Θ is the scattering angle, M_A is the mass of the nucleus and ϵ is the electron energy.

In the PWBA and considering - for example - even-even nucleus, the form factor is written in terms of the charge density as the Fourier transform of the density

$$F(q) = 4\pi \int_0 r^2 j_0(qr) n(r) dr, \tag{4.30}$$

with j_0 spherical Bessel function of zero order. Then the charge density can easily be obtained by anti-transforming the (4.30)

$$n(r) = \frac{1}{2\pi^2} \int_0 j_0(qr) F(q) q^2 dq. \tag{4.31}$$

The equations described above are obviously defined on an infinite range of moment transferred. Unfortunately, the experimental measurements can be performed only in range of q and therefore are affected by greater uncertainties near the origin, where there is a high moment transferred.
In this way, charge densities of the protons of a nucleus are obtained, but the inverse problem of Kohn-Sham requires probability densities. Then a conversion is needed which will be described later.
Experimental determination of neutron density can occur by adronic scattering experiments. Due to the lack of knowledge of the scattering amplitudes by the nucleon-nucleon iteration, the obtained measurements suffer from greater uncertainty compared to those obtained from electronic scattering and are difficult to find. In the literature, it was possible to find an article [10] concerning proton-nucleus scattering at mediun energies (E $\approx 300\ MeV$). in this case, the incident protons have a sufficiently low energy to reduce the production of mesons, but low enough to be described in pulse approximation.

Parameterization *SoG* - Densities obtained from experimental evidences are proton charge densities. The Kohn-Sham equations, on the other hand, require density probability. To solve this problem, it is possible to parameterize the charge densities in order to obtain density probabilities. De Vries, in its publication [9], offers a choice of different parameterizations applied on a good collection of nuclei. For the development of the following model, the choice fell on the *Sum of Gaussian* (SoG) parameterization. The first justification of this choice is is that it is model-independent. Chapter 1 describes the potential of the harmonic oscillator, of which the analytical forms of eigenfunction and eigenvalue are known. In particular, the eigenfunctions have a Gaussian trend for large r

$$\psi(r) \propto e^{-r^2}. \tag{4.32}$$

This same trend also characterizes probability densities. Then the choice of a parameterization of this type is understandable. The SoG parameterization presented in the De Vries article and in Zenihiro article [10] for neutron density for ^{208}Pb, occurs by means of the sum of 12 gaussian characterized by a width γ defined as the smaller width of the peaks of the nuclear radial wave functions, obtained with the HF method

$$\gamma = (\frac{2}{3}\langle r^2 \rangle)^{\frac{1}{2}}, \tag{4.33}$$

with $< r^2 >$ average quadratic radius of the involved nuclei

$$\langle r^2 \rangle = \frac{4\pi}{Ze} \int n(r) r^4 dr. \tag{4.34}$$

Thanks to rapid trend of the Gaussian tails, the contributions of the different functions that compose $n(r)$ are rather decoupled and this is an advantage.
Ultimately, the parameterization is implemented via

$$n(r) = \frac{N}{2\pi^{\frac{3}{2}}\gamma^3} \sum_i \frac{Q_i}{1 + 2\frac{R_i^2}{\gamma^2}} e^{-(\frac{r-R_i}{\gamma})^2} + e^{-(\frac{r+R_i}{\gamma})^2}. \tag{4.35}$$

The parameter Q_i represents the charge fraction contained in the i-th gaussian. The standardization criterion must be valid

$$\sum_i Q_i = 1 \tag{4.36}$$

The parametrization (4.35), is meant to provide the particle density distribution only in the case of neutrons extracted from p-scattering experiment of the ^{208}Pb as reported in [10]. For data from electron scattering, on the other hand, it provides the proton charge density. However, the proton is not a point particle and therefore the charge density and the probability density are linked to each other by the convolution of the proton form factor

$$n_{ch}(\overrightarrow{r}) = \int n(\overrightarrow{r}') n_{proton}(\overrightarrow{r} - \overrightarrow{r}') dr, \tag{4.37}$$

with n_{proton} being the proton. To reverse this equation and determine the probability density, it is useful to switch to the Fourier space by antitrasforming the quantity

$$\widetilde{n}(\overrightarrow{q}) = \frac{\widetilde{n}_{ch}(\overrightarrow{q})}{\widetilde{n}_{proton}(\overrightarrow{q})}. \tag{4.38}$$

For a proton shape factor defined for a Gaussian width of $\alpha = \sqrt{\frac{2}{3} < r_p >^2}$, we get

$$n_{proton}(r) = \frac{q_e}{\alpha^3 \pi^{\frac{3}{2}}} e^{-\frac{r^2}{\alpha^2}}, \tag{4.39}$$

from which we reach a density for protons given by

$$n(r) = \sum_i \frac{A_i}{2q_e\pi^{\frac{3}{2}}\beta r}[(\frac{r-R_i}{\beta^2} + \frac{R_i}{\gamma^2})e^{-\frac{(r-R_i)^2}{\beta^2}} + (\frac{r+R_i}{\beta^2} - \frac{R_i}{\gamma^2})e^{-\frac{(r+R_i)^2}{\beta^2}}], \tag{4.40}$$

where the coefficients A_i are defined as

$$A_i = \frac{NQ_i}{1 + 2\frac{R_i^2}{\gamma^2}}, \tag{4.41}$$

and with $\beta = \sqrt{\gamma^2 - \alpha^2}$. The R_i and Q_i parameters are those reported in the [9] and [10] articles.

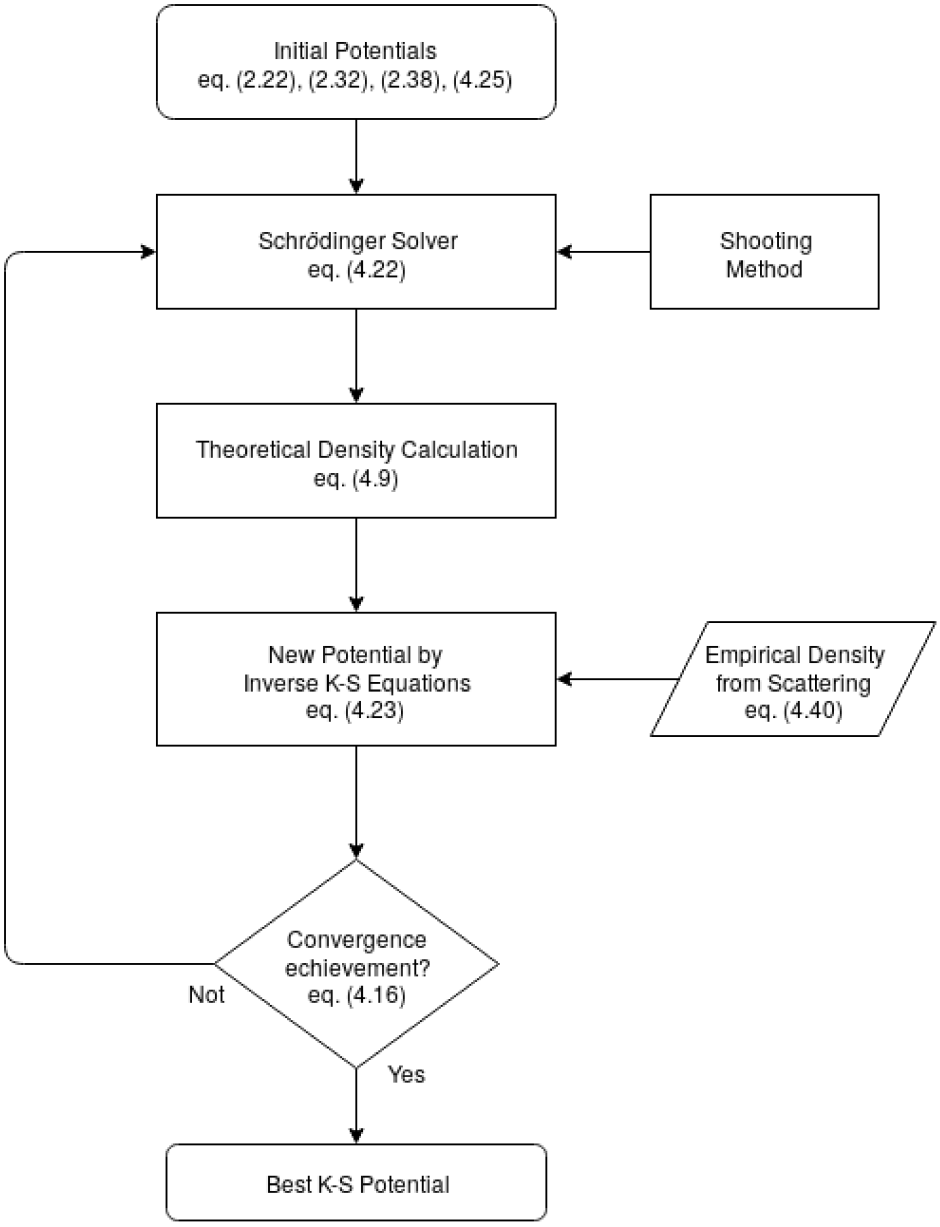

Figure 4.2: Model's block diagram. In each block, the equations used are specified.

Chapter 5

Results

In this chapter the main results obtained by applying the inverse problem to the Kohn-Sham equations using the inversion method vLB will be reported.

In order to explore the potentiality of the inversion algorithm as much as possible, at this stage, it was decided to focus the attention on three particular nuclei representative of different mass region. In particular, the attention fell on the ^{16}O for light nuclei, on the ^{40}Ca for medium-size nuclei and on the ^{208}Pb for heavy nuclei. It is no coincidence that the selected nuclei are characterized by being magical nuclei. This puts us in the condition in which all observables are able to analyze nuclides having closed shells, that is to be able to exploit a spherical symmetry independent of angular quantities but dependent only on the radial coordinate (as already shown with more detail in the previous chapter) and the effects of pairing are irrelevant. In addition, the magic nuclei, and especially the doubly magical ones like the ^{16}O, ^{40}Ca and the ^{208}Pb, enjoy greater stability than other neighbouring systems. To further simplify the model and further enhance the potentiality of the algorithm in use, it was decided not to include the spin-orbit term, whose presence has an effect that can be seen only on the eigenvalues, while it is negligible in the generation of eigenfunctions and consequently on the potential that is obtained from the inversion process. The spin-orbit term was added to the initial potential only for energetic evaluations of the orbital involved.

As already anticipated in the previous section, the literature provides only the proton charge density through the parameterization $_{12}SoG$ through the De Vries collection [9], therefore the results that will be shown will give greater prominence to the proton case only, while the neutron context will be presented only for completeness, exploiting the same De Vries parametrization assuming that the neutron density is very close to that of the protons for $N = Z$ nuclei. In any case, it is possible to deduce the neutron

density starting from the proton density by

$$n_N(r) = \frac{N}{Z} n_P(r). \tag{5.1}$$

For the sole case of the ^{208}Pb it is also possible to refer to the specific parameterization for neutrons, thanks to the work of Zenihiro [10], thus allowing to obtain more accurate and complete evaluations.
For all the simulations carried out, it was decided to use the potential of Woods-Saxon as initial potential in the iterative process with standard parametrization (potential depth V_0 given by (2.34), nuclear radius equal to (2.33) and the thickness of the nuclear surface equal to $a_0 = 0.67\ fm$). For the study of protons, the Coulomb contribution given by (2.38) was added to the initial potential. It is useful to remember that, in the DFT, the potential has a fully determined structure except for an arbitrarily large constant term.

5.0.1 Density and potentials from the vLB method

In this section, the potentials shown in the figures have been traslated by a constant, which is legitimate, and the translation reads

$$U_{KS} - E_{KS} + E_{exp}, \tag{5.2}$$

where U_{KS} is the Kohn-Sham potential, E_{KS} and E_{exp} are the absolute value of the single-particle energies, obtained and experimental respectively.

^{16}O **Nucleus** - Representing the light nuclei, the ^{16}O has 8 neutrons and 8 protons that are arranged in turn on the first three orbitals of the shell model $1s_{1/2}$, $1p_{3/2}$ and $1p_{1/2}$ filling them completely. The density and potential associated with it, obtained by the inversion algorithm of the Kohn-Sham equations, were obtained by keeping the ϵ parameter of the convergence criterion equal to 1% of the target density value and exploring a maximum radius of $3R_n$.
As the following figures show, a first demonstration of the potentiality of the inversion algorithm is given by the Kohn-Sham density obtained at the end of the inversion process and which reflects the empirical one determined by the parameterization $_{12}SoG$. The figures 5.1 and 5.2 shows precisely how, aside from two negligible imperfections at about 0.5 fm and 1.2 fm, the density obtained faithfully overlaps the

curve relative to the target density.

The form of the Kohn-Sham potential which results from the inversion, is not as appreciable as that of the density associated with it. While maintaining a Woods-Saxon shape, the figure 5.4 shows a curve that presents sudden depressions that characterize the entire radial interval. As for all light nuclei, the ^{16}O is characterized by a very large surface compared to its density and also due to the low number of investigable states, the vLB method is subject to a first limit that compromises the prediction of a potential close to the real one.

In the table 5.1, the single particle energy obtained from the inversion is reported and compared with the experimental data.

Table 5.1: Single particles energies for ^{16}O. Energies are reported in [MeV]. Experimental values from Vautherin and Brink [1].

	Protons		Neutrons	
Level	Experimental value	Present work	Experimental value	Present work
$1s_{1/2}$	-	-28.0004	-	-31.9907
$1p_{3/2}$	-18.4	-13.0552	-21.84	-17.0602
$1p_{1/2}$	-12.13	-14.3563	-15.66	-18.3631

The single-particle energies reproduced by the developed model show evident discrepancies compared to the experimental values. The origin of these differences is to be found in two distinct causes. A first aspect that may have negatively influenced the estimated energies is represented by the Coulomb interaction used. In the developed model, it assumes an excessively approximate analytical form (2.38). A second cause could be due to have neglected possible effects from density gradient-dependent interactions. Also, it is good to remember that, in DFT, the single-particle energies are mainly auxiliary quantities. It is, therefore, natural to not expect that the model is not able to reproduce them more accurately.

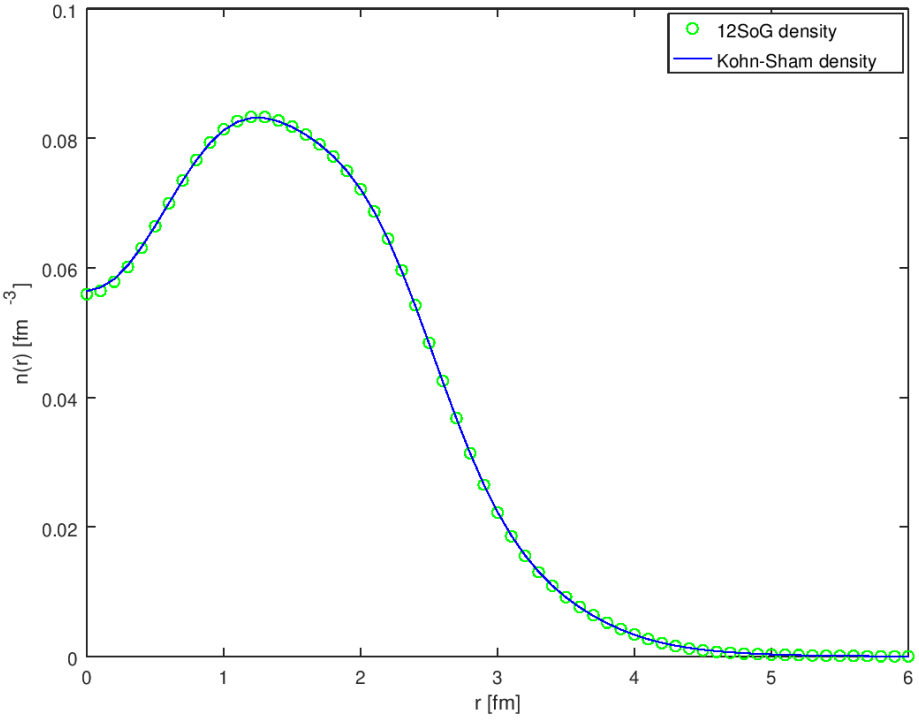

Figure 5.1: Neutron density at convergence achieved for ^{16}O.

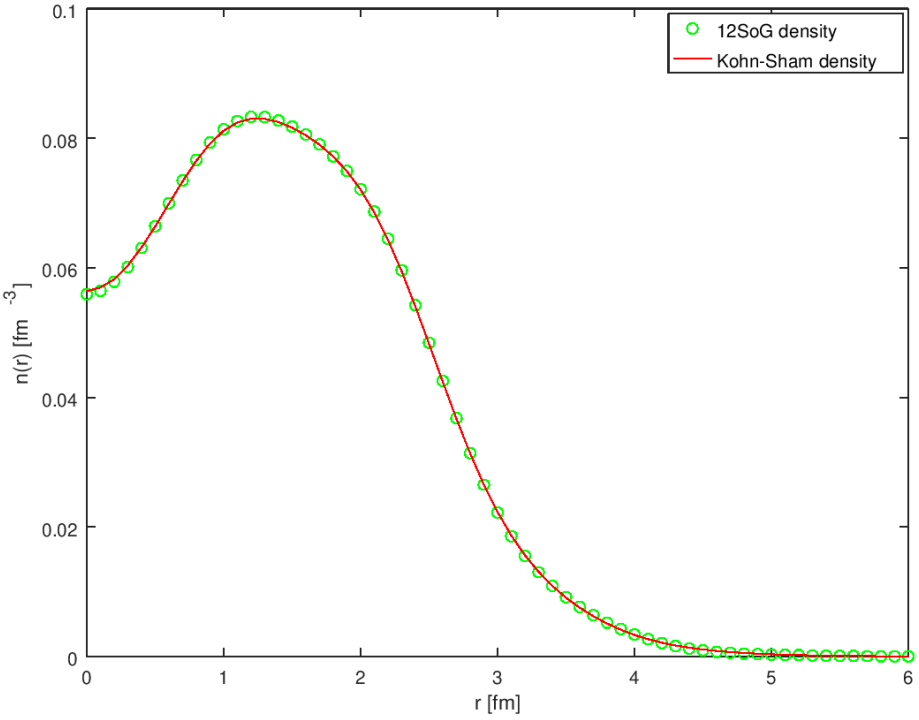

Figure 5.2: Proton density at convergence achieved for ^{16}O.

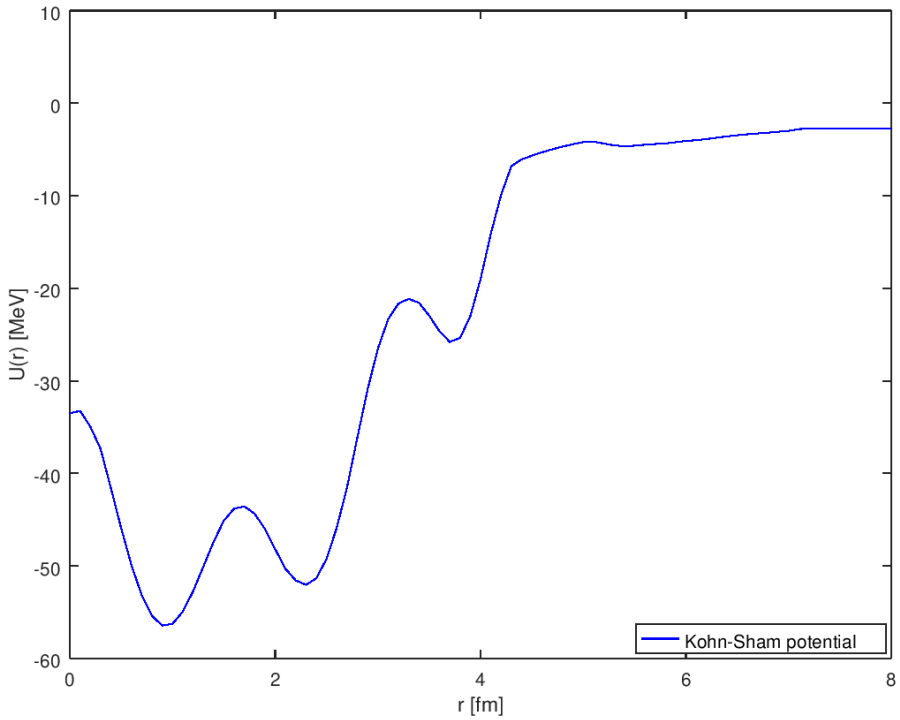

Figure 5.3: Neutron Kohn-Sham potential at convergence achieved for ^{16}O.

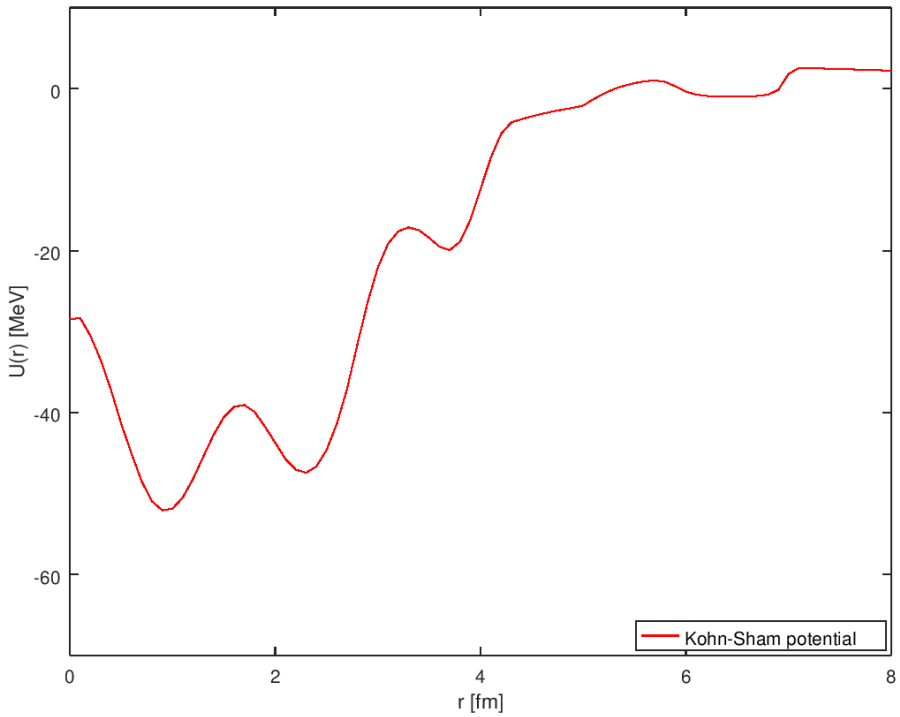

Figure 5.4: Proton Kohn-Sham potentia at convergence achieved for ^{16}O.

^{40}Ca **Nucleus** - Formed by 20 neutrons and 20 protons, the ^{40}Ca is a doubly magic one that represents the category of medium-size nuclei. Its nucleons are arranged to completely fill the $1s_{1/2}$, $1p_{3/2}$, $1p_{1/2}$, $1d_{5/2}$, $2s_{1/2}$ and $1d_{3/2}$ states. Also in this case, the convergence criterion was respected by imposing a value ϵ equal to 1% of the value of the target density and exploring a region characterized by a maximum radius of $3R_n$.

The figure 5.5 shows, in the proton case, how the density obtained faithfully follows the curve of the target density and only for a first region to about 0.8 fm a slight and negligible underestimation of the obtained result can be detected. Even in the neutron case (figure 5.6) it is possible to appreciate how the curve obtained is superimposed on the parameterized $_{12}SoG$ one and only a negligible underestimation is visible in the $[1 - 2.8\ fm]$ range.

In this case, the potentials obtained by the inversion algorithm are comparable with those obtained by the HF method and are characterized apart from the irregularities on the tail. The origin of this behavior has a numerical nature dictated by an intrinsic limit of the inversion algorithm since, as will be shown later in the discussion, these irregularities can be mild or even vanish according to the parameterization used and the number of states studied.

Also in this case, the energies of a single-particle are shown in table 5.2.

Table 5.2: Single particles energies for ^{40}Ca. Energies are reported in [MeV]. Experimental values from Vautherin and Brink [1].

	Protons		Neutrons	
Level	Experimental value	SPresent work	Experimental value	Present work
$1s_{1/2}$	-	-28.3455	-	-37.3374
$1p_{3/2}$	-	-18.3194	-	-27.3033
$1p_{1/2}$	-	-19.0018	-	-27.9844
$1d_{5/2}$	-15.07	-7.66504	-22.39	-16.6162
$2s_{1/2}$	-10.92	-6.32658	-18.19	-15.2237
$1d_{3/2}$	-8.33	-3.38329	-15.64	-12.3288

Also in this case, there are evident differences between the predicted single-particle energies and the experimental ones. The values obtained for the protons are more underestimated. This, further supports the hypothesis made in the previous case on the possible cause due to the approximate Coulomb interaction.

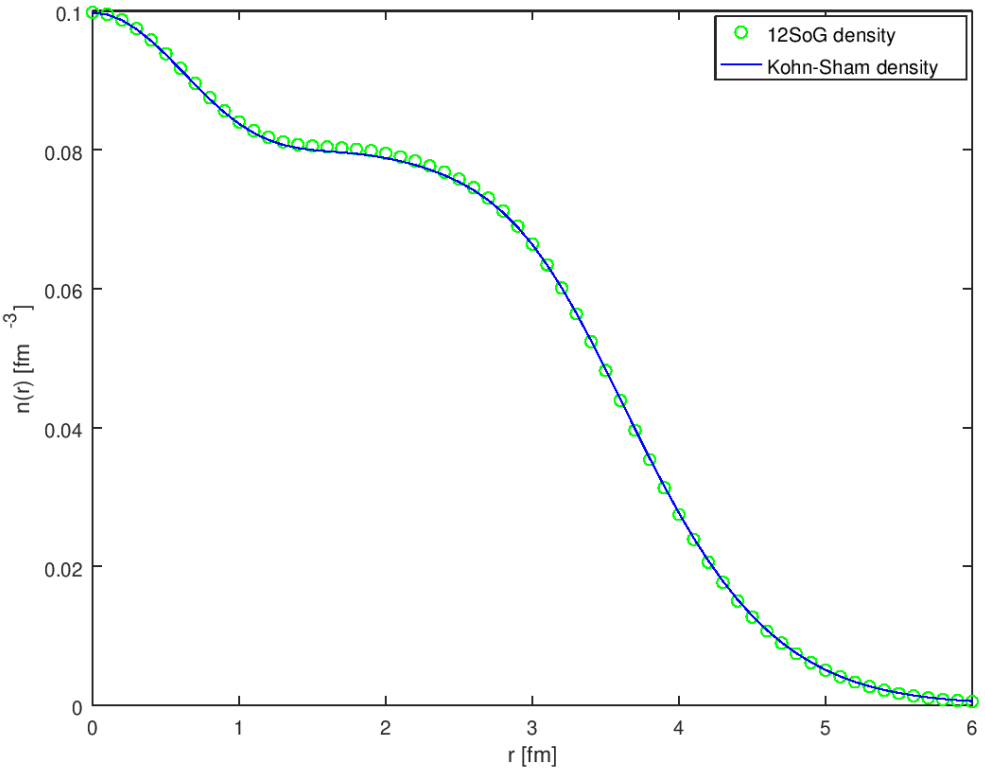

Figure 5.5: Neutron density at convergence achieved for ^{40}Ca.

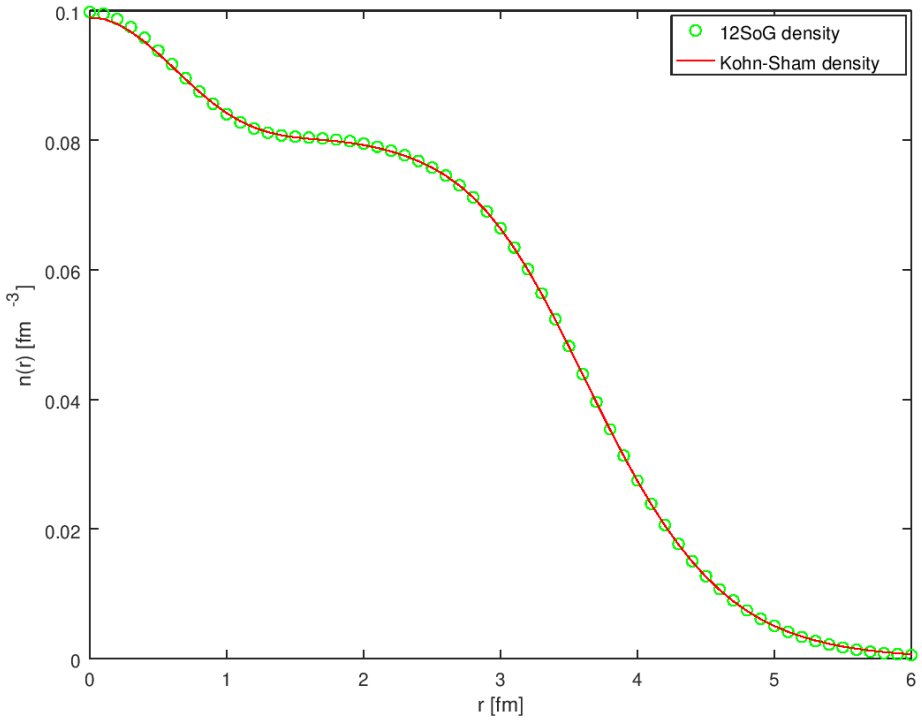

Figure 5.6: Proton density at convergence achieved for ^{40}Ca.

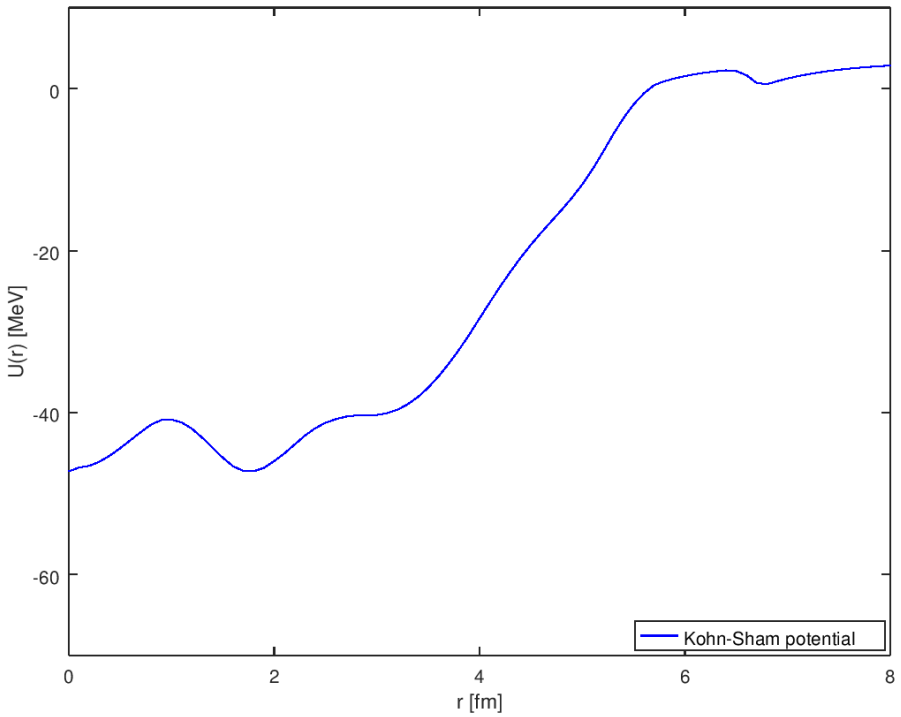

Figure 5.7: Neutron Kohn-Sham potential at convergence achieved for ^{40}Ca.

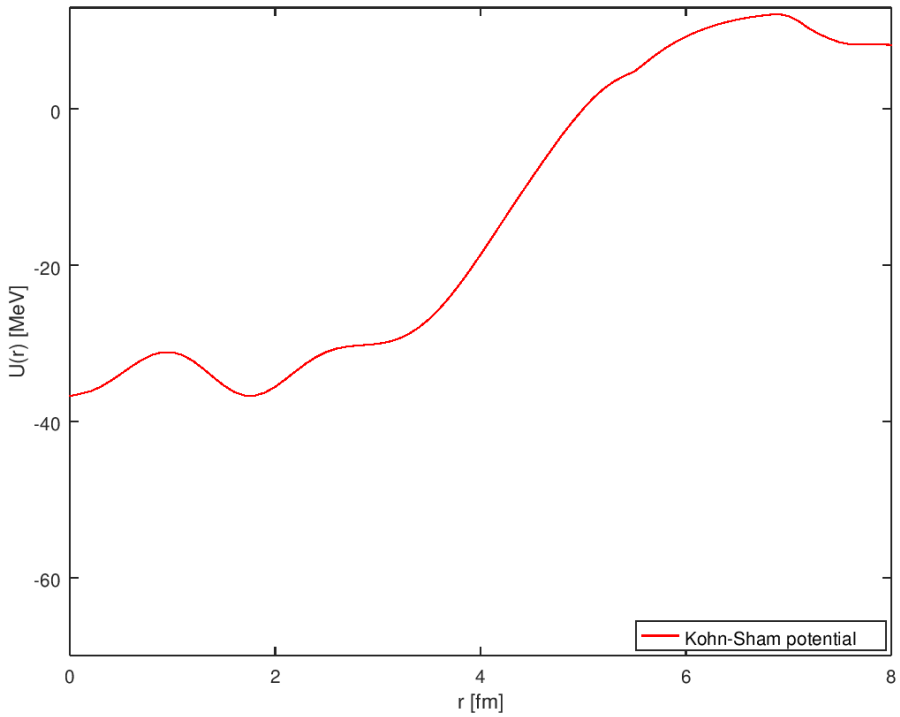

Figure 5.8: Proton Kohn-Sham potential at convergence achieved for ^{40}Ca.

^{208}Pb **Nucleus** - Among the heavy nuclei, the ^{208}Pb is the most studied and there is a huge literature on it. As we will see, it also allows a better determination of the potential from the vLB method. The large number of nucleons arranged on a greater number of energy levels (22 orbital for the 126 neutrons, 16 orbital for the 82 protons) implies, by the model, a heavier computational work, but which leads to a marked improvement of the results.

Unlike the previous cases examined, for the achievement of convergence it was appropriate to differentiate the parameters required by the model, not only with respect to the other nuclei so far treated. Specifically, to maintain the value of ϵ equal to 1% of the target density value (both protonic and neutronic), it was necessary to vary the maximum integration radius to $2R_n$. Maintaining a maximum radius of $3R_n$ would oblige to set a ϵ equal to 5% of the target density value, thus leading to less accurate results.

The figures 5.9 and 5.10, show how also in this case the solution to the direct problem leads to a good reproduction of the densities. Both for protons and for neutrons, the curve of the obtained density superimposes that of the density $_{12}SoG$, only for values of r less than 0.5 fm it is possible to notice a slight and negligible underestimation for neutrons and overestimation for protons.

As already mentioned, the high computational workload of the inversion algorithm allows to obtain potentials characterized by much better tails than the counterparts of the previous cases. The figures 5.11 and 5.12, show how in the case of heavy nuclei, such as the ^{208}Pb, the trend in the tail of the

potentials is much more regular and free from the irregularities found in the cases of lighter nuclei. This result brings to light a first limit of the vLB method, resulting particularly dependent on the parameters of convergence and making it more effective with regard to the heavy nuclei rather than those of small and medium size. In any case, the results obtained so far demonstrate how the vLB method is more performing in the case of heavy nuclei, that is when there is a configuration in which there is a predominance of volume in comparison to the surface.

For the ^{208}Pb energies are shown in the following table

Table 5.3: Single particles energies for ^{208}Pb. Energies are reported in [MeV]. Experimental values from Vautherin and Brink [1].

	Protons		Neutrons	
Level	Experimental value	Present work	Experimental value	Present work
$1s_{1/2}$	-	-24.7797	-	-40.4654
$1p_{3/2}$	-	-21.2682	-	-36.7009
$1p_{1/2}$	-	-21.3717	-	-36.7966
$1d_{5/2}$	-	-16.7611	-	-32.0613
$1d_{3/2}$	-	-16.0352	-	-31.385
$2s_{1/2}$	-	-14.1852	-	-30.0641
$1f_{7/2}$	-	-11.3902	-	-26.5458
$1f_{5/2}$	-	-10.0006	-	-25.2444
$2p_{3/2}$	-	-7.73651	-	-22.8802
$2p_{1/2}$	-15.07	-7.91502	-	-23.0515
$1g_{9/2}$	-15.43	-5.28429	-	-20.2862
$1g_{7/2}$	-11.43	-3.01914	-	-18.1474
$2d_{5/2}$	-9.70	-0.9908	-	-16.006
$1h_{11/2}$	-9.37	1.45189	-	-13.4112
$2d_{3/2}$	-8.38	0.14749	-	-14.8679
$3s_{1/2}$	-8.03	0.37824	-	-15.6275
$1h_{9/2}$	-	-	-10.85	-10.2071
$2f_{7/2}$	-	-	-9.72	-9.14238
$1i_{13/2}$	-	-	-9.01	-6.05926
$3p_{3/2}$	-	-	-8.27	-7.81959
$2f_{5/2}$	-	-	-7.95	-7.11575
$3p_{1/2}$	-	-	-7.38	-8.0567

Unlike previous cases, for ^{208}Pb neutrons, the single-particle energies obtained are less underestimated than those related to protons. The surface of a heavy nucleus takes on less importance than its volume. Then it is appropriate to think that density gradient-dependent terms affects more the energies of light nuclei.

For the case of ^{208}Pb only, a further test was taken into consideration to evaluate the reliability of the inversion algorithm. We wanted to reproduce a potential starting from the target densities generated by an HF simulation. It is expected that the target HF potential is compatible with the analogue produced by the vLB method.

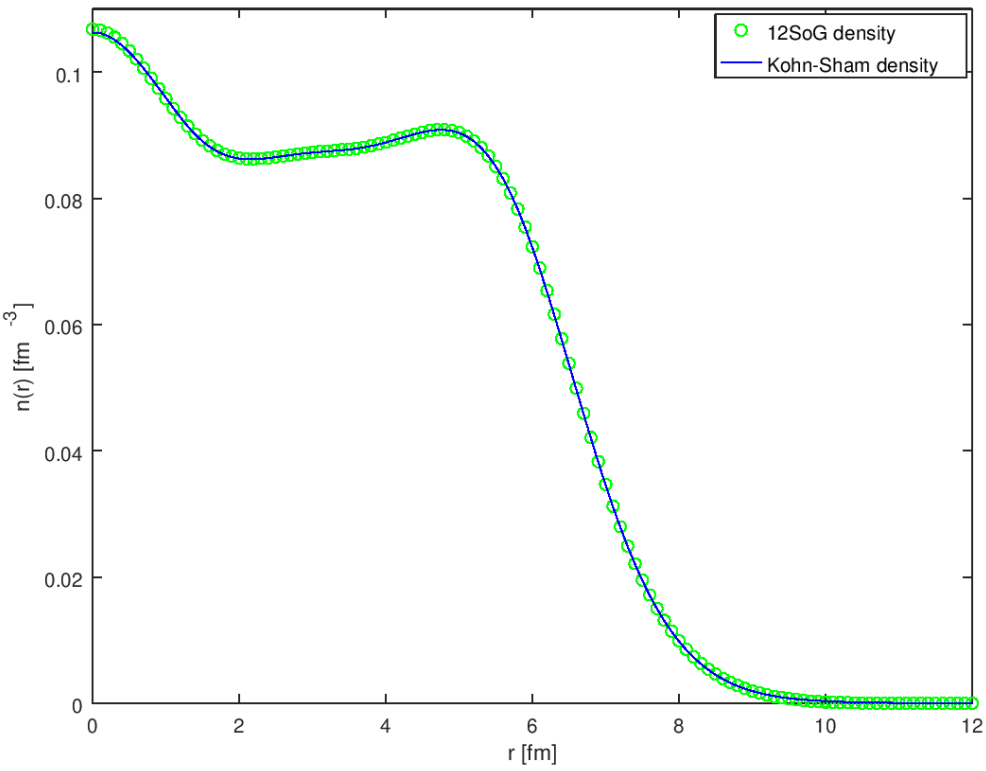

Figure 5.9: Neutron density at convergence achieved for ^{208}Pb.

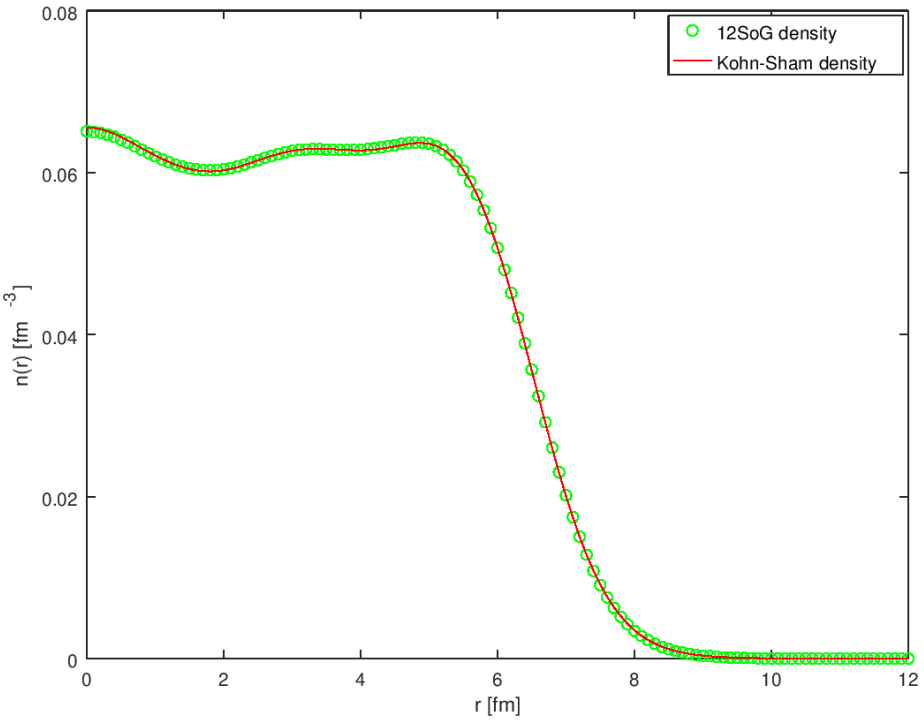

Figure 5.10: Proton density at convergence achieved for ^{208}Pb.

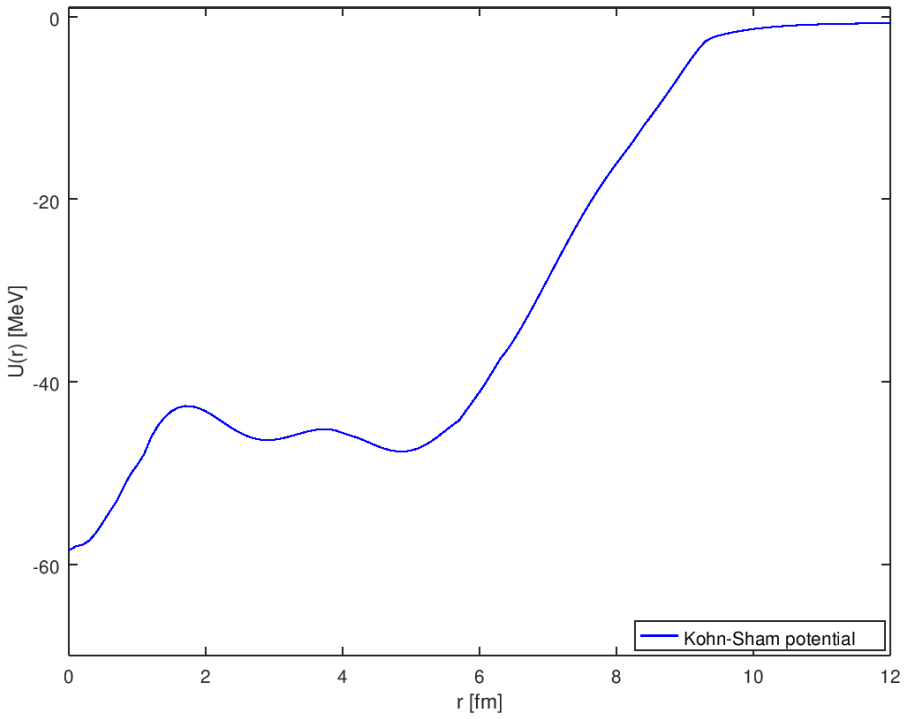

Figure 5.11: Neutron Kohn-Sham potential at convergence achieved for ^{208}Pb.

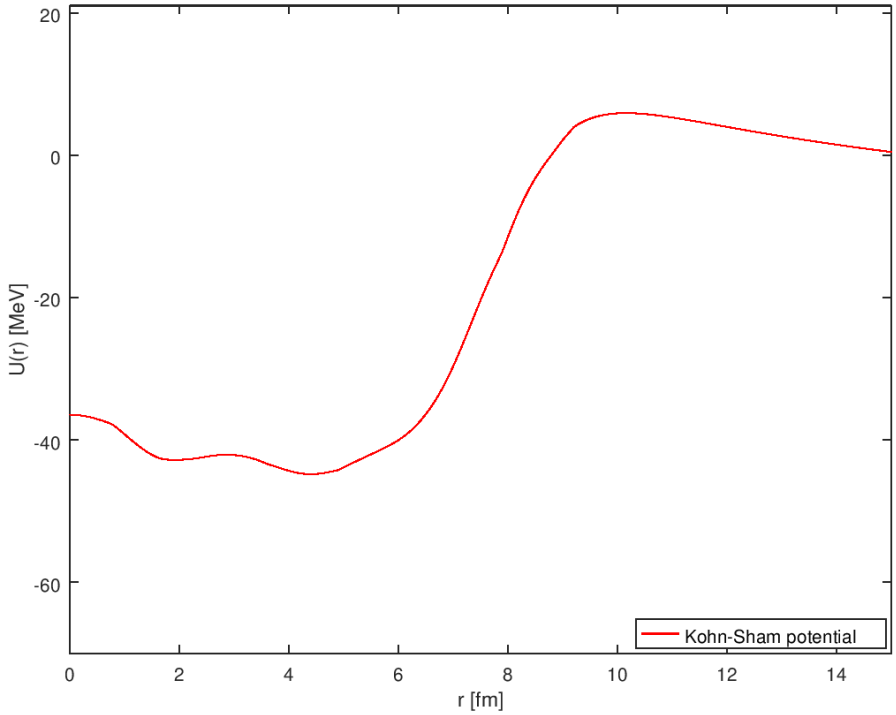

Figure 5.12: Proton Kohn-Sham potential at convergence achieved for ^{208}Pb.

The HF target density and its relative potential were obtained by the Skyrme SKP parameter set on a number of points and meshes of 200 and 0.1 respectively. The contribution of the spin-orbit interaction was not considered.

Figures from 5.13 to 5.16 show the potentials and densities obtained for neutrons and protons with substantial differences. In both cases, neutron and proton, the vLB method is able to replicate the target density with a negligible error, and in particular the proton density obtained overlaps almost perfectly the density from the HF calculation. The potentials deriving from it, on the other hand, are characterized by evident shape changes. For neutrons, an underestimation of about 10 MeV is obtained at the origin. Subsequently, the potential follows roughly the trend of the corresponding HF. On the contrary, the protonic potential obtained is abundantly overestimated throughout the inner region, although maintaining the shape of the HF potential and overlapping it only on the surface.

5.0.2 The initial potential in the vLB method

Generally, any self-consistent numerical method should be able to return a result regardless of the initial data used to allow the process to start. The results so far obtained and discussed have brought out the

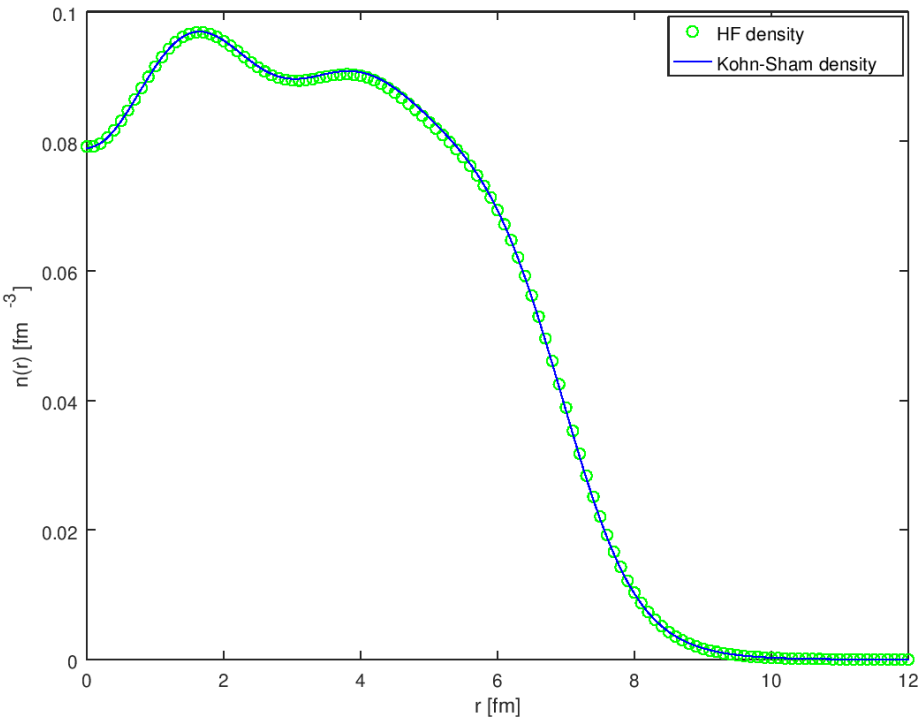

Figure 5.13: Comparison between Kohn-Sham neutron density and Hartree-Fock neutron density for ^{208}Pb.

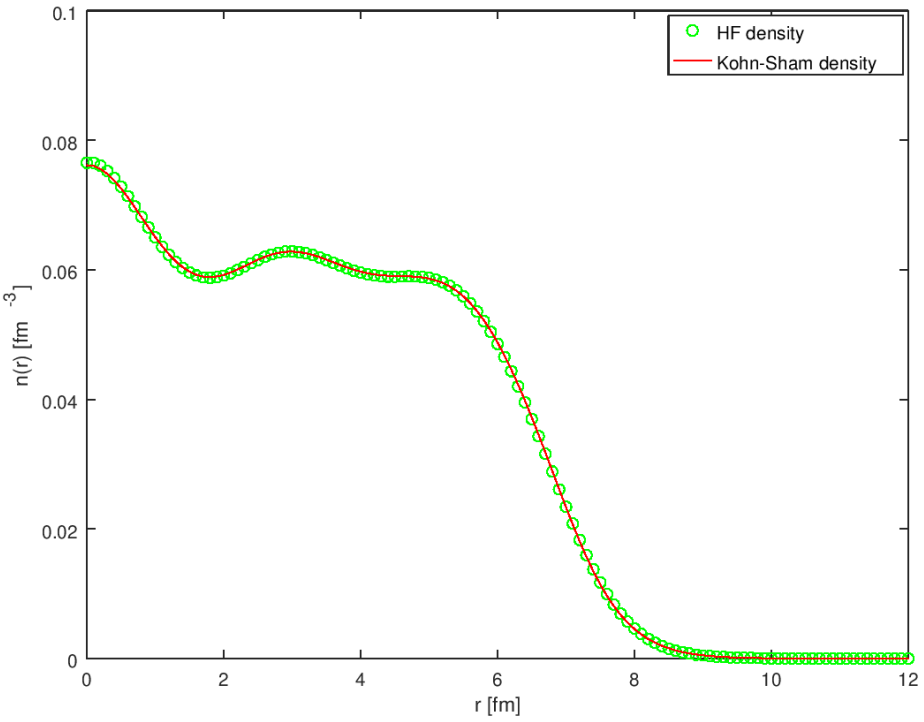

Figure 5.14: Comparison between Kohn-Sham proton density and Hartree-Fock proton density for ^{208}Pb.

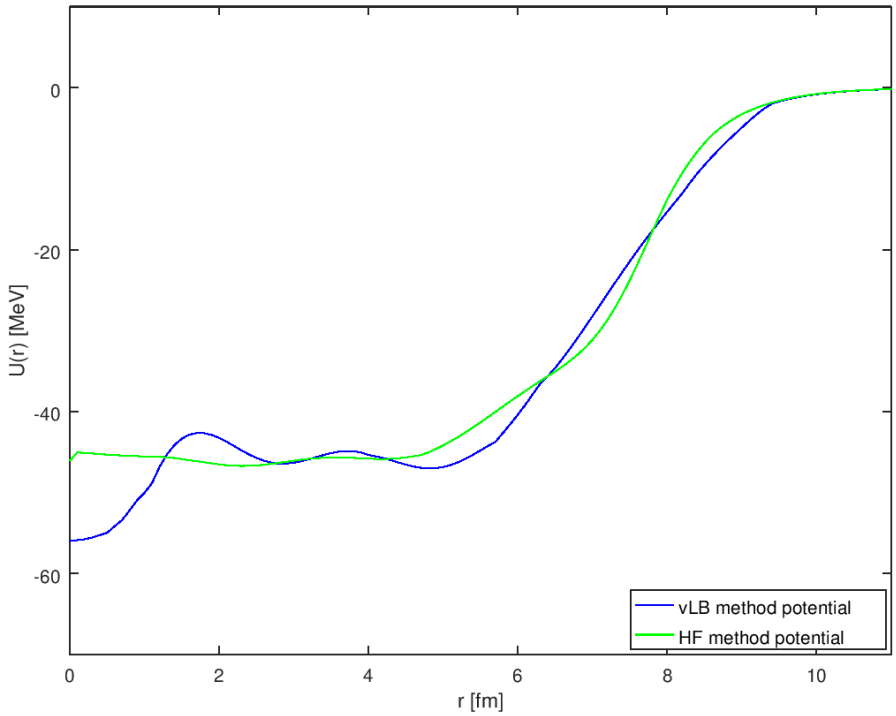

Figure 5.15: Comparison between Kohn-Sham neutron potential and Hartree-Fock neutron potential for ^{208}Pb.

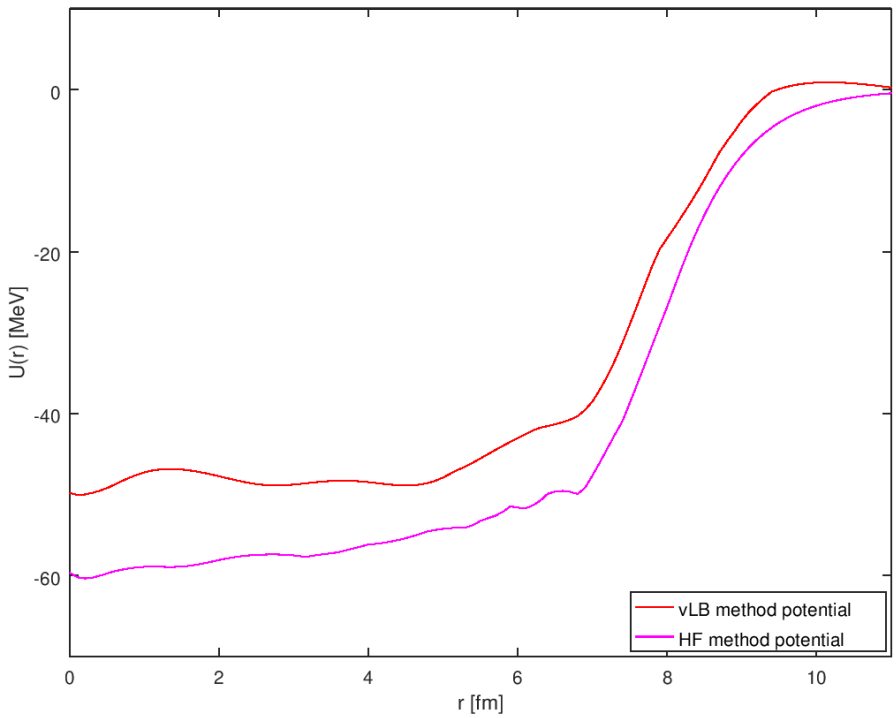

Figure 5.16: Comparison between Kohn-Sham proton potential and Hartree-Fock proton potential for ^{208}Pb.

limitations of the vLB method studied here and a further step forward in testing the inversion algorithm consisted in varying the initial potential. For the previous cases, the potential of Woods-Saxon has always been exploited as initial potential through the classic parameterization as reported in the literature and defined by the equations (2.34) and (2.33) with $a_0 = 0.67\ fm$, while for this new attempt it was decided to rescale the aforementioned potential. For simplicity of work, we have opted to study only the medium-size nuclei represented once again by the ^{40}Ca and paying attention only to the neutron case, in order to better evaluate the changes due to a change in the initial data and that could somehow be masked by the presence of the Coulomb term.

A first attempt at rescaling the initial potential consisted of setting the depth equal to $V_0 = 10MeV$ and the nuclear radius to $R_n = 10\ fm$ and then rescaling with $V_0 = 50\ MeV$ and $R_n = 1\ fm$. In both cases, and once again, the obtained densities result to describe the target densities with good precision, while the potentials assume - in the innermost region - the same form of the counterparts discussed in the previous paragraph. Now, the behavior in tail with less numeric noise is improved, but a lower depth of potential is highlighted.

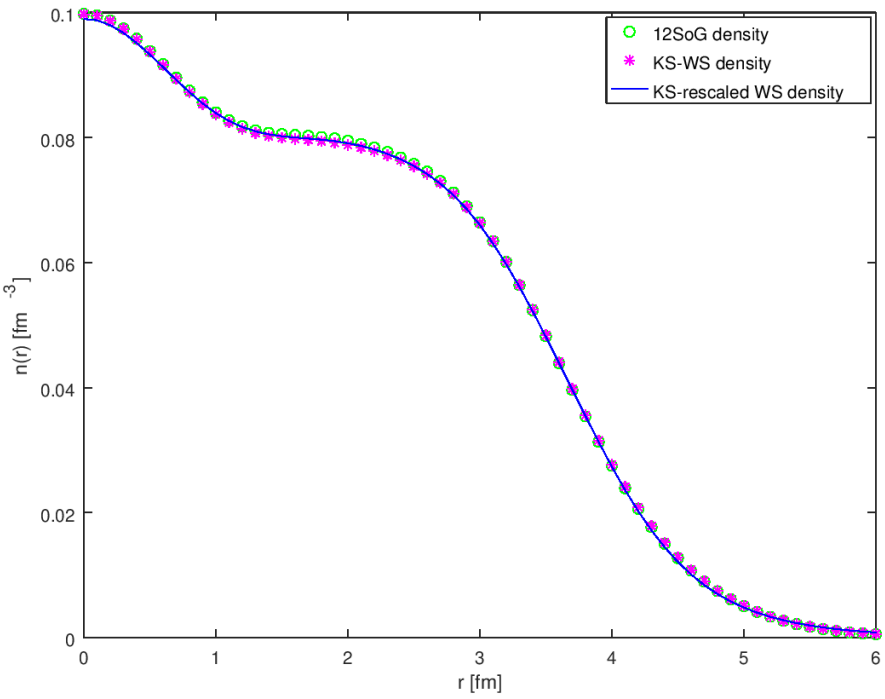

Figure 5.17: Neutron densities in rescaled Wood-Saxon initial potential case with $V_0 = 10MeV$ and $R_n = 10fm$ for ^{40}Ca case.

Any other attempt to recover the initial potential with a value of V_0 greater than what is defined by (2.34), leads to non-convergence, even increasing the value of ϵ in the convergence criterion and again,

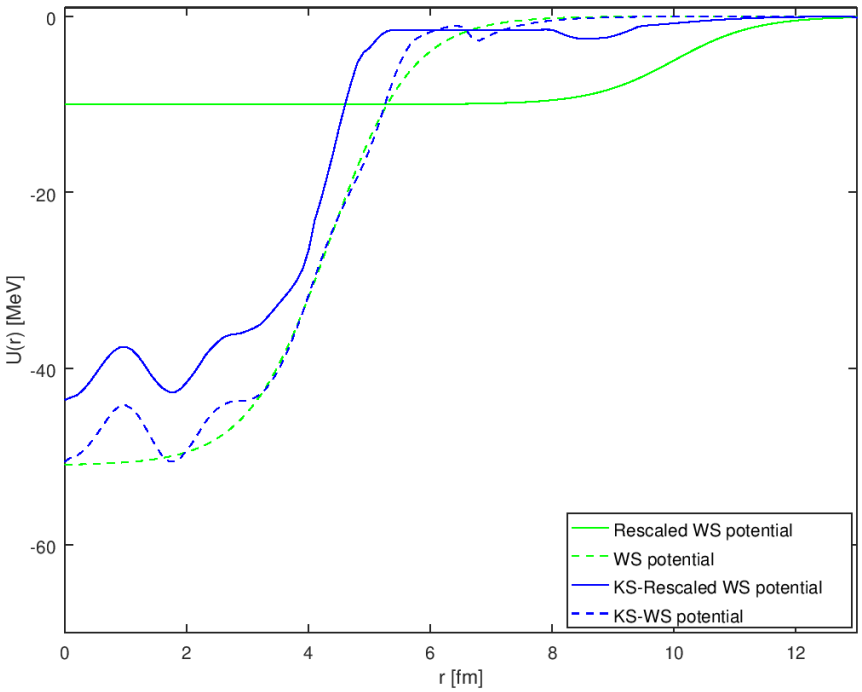

Figure 5.18: Comparison between the Kohn-Sham potential obtained from a rescaled Wood-Saxon potential with $V_0 = 10MeV$ and $R_n = 10fm$ (continuous line) and the Kohn-Sham potential obtained from the Wood-Saxon potential with regular parametrization (dotted line) for ^{40}Ca neutron case.

the inversion algorithm (4.23) proves to be fragile in certain contexts.

In addition to what has already been done, the replacement of the initial potential of Wood-Saxon with the harmonic oscillator potential defined as in (2.22), leads to highlight the major problems of the inversion algorithm. The use of an initial potential of this form has led to results hardly comparable to those shown so far. The theoretical densities obtained from the resolution of the direct problem, despite being compatible with the target ones, are affected by slight inaccuracies, as opposed to what obtained using an input Wood-Saxon potential. The potentials associated with them present obvious anomalies due to numerical noise, which, as regards the light nuclei, completely distorts the shape making it impossible to perform any physical interpretation. For medium and heavy nuclei, although in the internal regions they assume a probable shape, the greatest problems have been obtained on the tails, completely distorted by numerical errors. Moreover, by examining several nuclei (which are not mentioned in the present work) a certain degree of difficulty is determined, if not impossible, to find a parametric configuration suitable for achieving convergence.

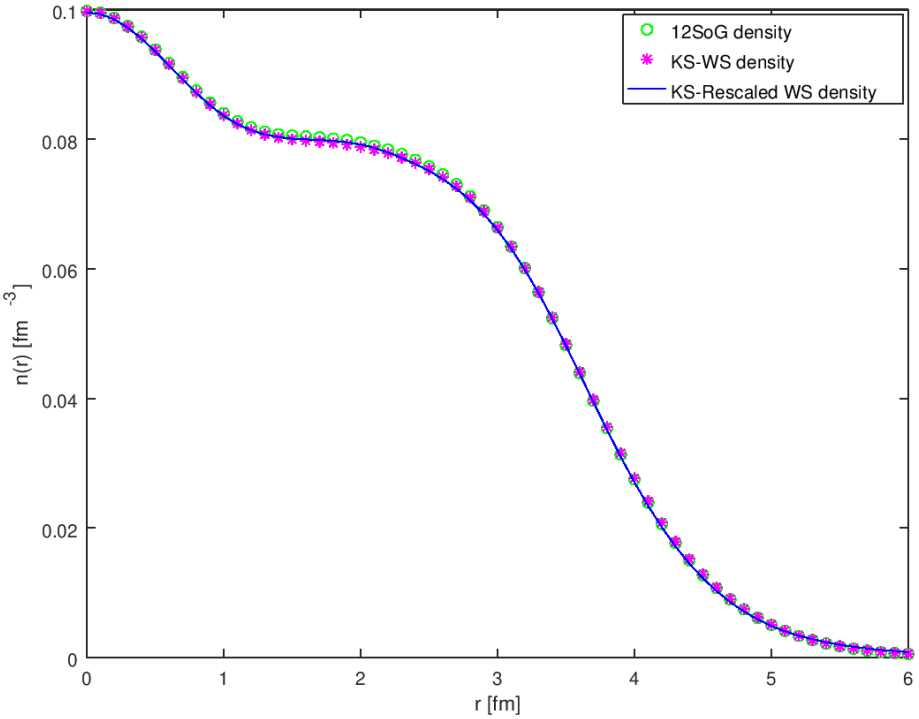

Figure 5.19: Neutron densities in rescaled Wood-Saxon initial potential case with $V_0 = 50MeV$ and $R_n = 1fm$ for ^{40}Ca case.

5.0.3 Comparison between the vLB method and the CV method

Up to now, the results obtained from the model developed have been presented and an evaluation has been given with reference to what is known in nuclear physics and reported in the literature. As we have seen, the vLB method finds its best performance in simulations involving heavy nuclei. For this reason, only for ^{208}Pb the results were compared with those produced by a Hartree-Fock simulation.

A further way to verify the goodness of what is produced by the inversion method vLB, consists in making a comparison with the solutions of the inverse problem of Kohn-Sham by a different inversion method. Two inversion procedures of different nature generate numerical error in different ways and quantities. Of course, we do not expect to find the same results, but they are at least in agreement. For this comparison, we relied on results from a mathematical model based on a constrained variational method (CV) for the solutions of the inverse problem. A brief description of the CV method is required.

The vLB method provides for the solution of an eigenvalue problem at each step of the iterative process. For light and medium-size nuclei, this procedure is not too challenging, but for heavy cores the computational load becomes important. Levy's constrained search can be used directly to implement a density-to-potential inversion method without the need to solve the problem of each iteration of the

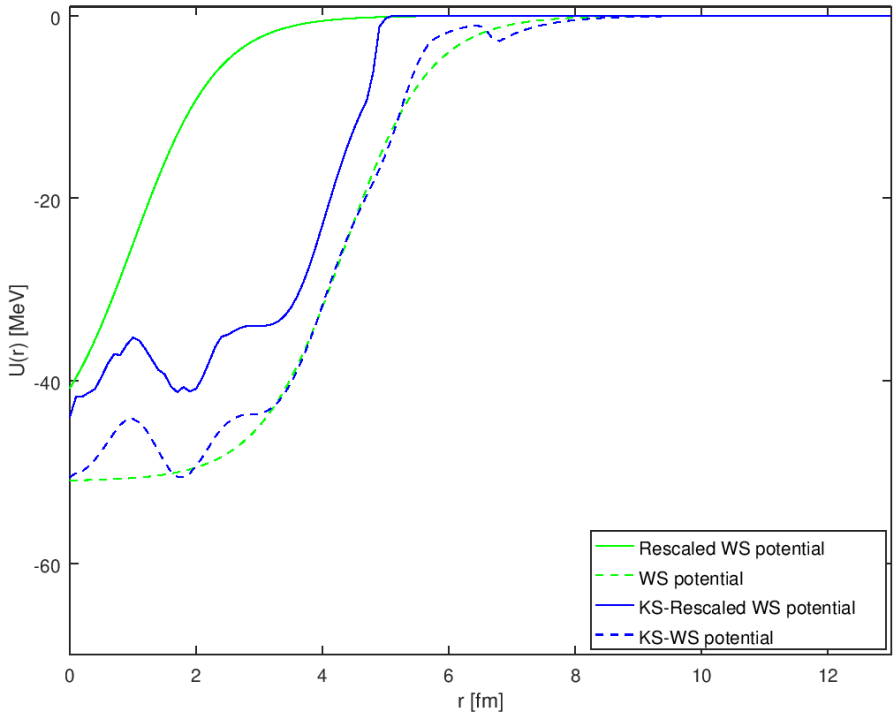

Figure 5.20: Comparison between the Kohn-Sham potential obtained from a rescaled Wood-Saxon potential with $V_0 = 50MeV$ and $R_n = 1fm$ (continuous line) and the Kohn-Sham potential obtained from the Wood-Saxon potential with regular parametrization (dotted line) for ^{40}Ca neutron case.

process. In the approximation of non-interacting particles, in the CV method the minimization of kinetic energy is performed placing the constraint of the orthonormality to the orbitals. The functional to be minimized makes use of the Lagnage multipliers

$$\begin{aligned} f[\phi_j] &= -\frac{\hbar^2}{2m}\int d^3r \sum_{j=1}^{N} \phi_j^*(\overrightarrow{r})\nabla^2\phi_j(\overrightarrow{r}) \\ &= -\frac{\hbar^2}{2m}\int d^3r \sum_{j=1}^{N} [\nabla(\dot{\phi_j^*}(\overrightarrow{r})\nabla\phi_j(\overrightarrow{r})) - |\nabla\phi_j(\overrightarrow{r})|^2] \\ &= \frac{\hbar^2}{2m}\int d^3r \sum_{j=1}^{N} |\nabla\phi_j(\overrightarrow{r})|^2 \end{aligned} \tag{5.3}$$

where N is the number of filled orbitals. To justify the last equality, it is specified that the first term in the second line does not contribute if a boundary condition is set to infinity at wave functions. At this point, a density constraint is imposed and $N(N+1)/2$ constraints to the orthonormality

$$c_0(\overrightarrow{r}) = \sum_{j=1}^{N} |\phi_j(\overrightarrow{r})|^2 - n(\overrightarrow{r}) = 0 \tag{5.4}$$

$$c_{jk} = \langle\phi_j|\phi_k\rangle - \delta_{jk} = \int d^3r' \phi_j^*(\overrightarrow{r'})\phi_k(\overrightarrow{r'}) - \delta_{jk} = 0 \tag{5.5}$$

where $j = 1, ..., N$ and $k = 1, ..., N$ are adequate sets of quantum numbers. If Kohn-Sham's orbitals are considered real, one can define an auxiliary Lagrangian, took Lagrange's multipliers

$$\lambda_i = -\frac{\delta f[\phi_j]}{\delta c_i} \tag{5.6}$$

Then the constraint c_0 defined in (5.4) is connected to the Kohn-Sham potential from the

$$v_{KS}(\overrightarrow{r}) = -\frac{\delta f[\phi_j]}{\delta \sum_{j=1}^{N} |\phi_j(\overrightarrow{r})|^2} = -\frac{\delta}{\delta n} < \Phi_{KS}|\widehat{T}_{KS}|\Phi_{KS} > \tag{5.7}$$

Thus, defining a functional J, which is the auxiliary Lagrangiana, is obtained

$$J[\phi_j; v_{KS}(\overrightarrow{r}), \epsilon_{jk}] = \frac{\hbar^2}{2m}\int d^3r \sum_{j=1}^{N} |\phi_j(\overrightarrow{r})|^2 + \\ + \int d^3r v_{KS}(\overrightarrow{r})(\sum_{j=1}^{N} |\phi_j(\overrightarrow{r})|^2 - n(\overrightarrow{r})) + \\ + \int d^3r \sum_{j=1}^{N}\sum_{k=1}^{N} \epsilon_{jk}(\int d^3r' \phi_j^*(\overrightarrow{r'})\phi_k(\overrightarrow{r'}) - \delta_{jk}) \tag{5.8}$$

with ϵ_{jk} kinetic energy. Finally, the minimization process leads to

$$\frac{\hbar^2}{m}\int d^3r \phi_\beta(\overrightarrow{r})\nabla^2\phi_\alpha(\overrightarrow{r}) = 2\int d^3r[\phi_\beta(\overrightarrow{r})v_{KS}(\overrightarrow{r})\phi_\alpha(\overrightarrow{r}) + \\ + \int d^3r \phi_\beta(\overrightarrow{r})[\sum_{j=1}^{a}\phi_j(\overrightarrow{r})\epsilon_{ja} + \sum_{k=1}^{a}\epsilon_{ak}\phi_k(\overrightarrow{r}] \tag{5.9}$$

where $\alpha = 1, ..., N$ and $\beta \geqslant \alpha$. By solving these linear equations it is possible to obtain the Kohn-Sham potential. For further clarification, refer to the article [8].

The comparison between the vLB and CV inversion scheme was initially performed using a parameterized density ${}_{12}SoG$ as target density in both cases, protons and neutrons.

The figures 5.21 and 5.22, show how the densities obtained by both inversion methods are completely in agreement throughout the region explored with respect to the experimental density. Also potentials obtained, shown in the figures 5.23 and 5.24, take the same shape from the origin and throughout the central radial region up to about 8.3 fm. With the inversion vLB the expected tails are obtained, as clearly shown in the neutron case in which the tail is brought to zero in a regular way. The CV inversion, on the other hand, produces tails that follow the asymptotic trend inherited from the Gaussian sum parameterizations.

A further comparison between the two inversion schemes was carried out using target densities from previously used HF simulations. In this case, the VLB and CV densities are slightly overestimated in the central region from 4 fm to 6 fm, in the case of neutrons, and slightly underestimated at the origin in the case of protons (figures 5.25 and 5.26). The protons potentials predicted are in agreement over the whole radial interval (figure 5.28). The tiles of the vLB and CV potentials are different from the HF one, because the Coulomb interaction was considered for extraction of the first two but not for that of the HF potential. For neutrons, the CV scheme is able to produce a potential that matches HF, contrary to what was obtained with vLB and previously discussed (figure 5.27). For completeness, the figures also

show the HF potentials linked to the target densities used.

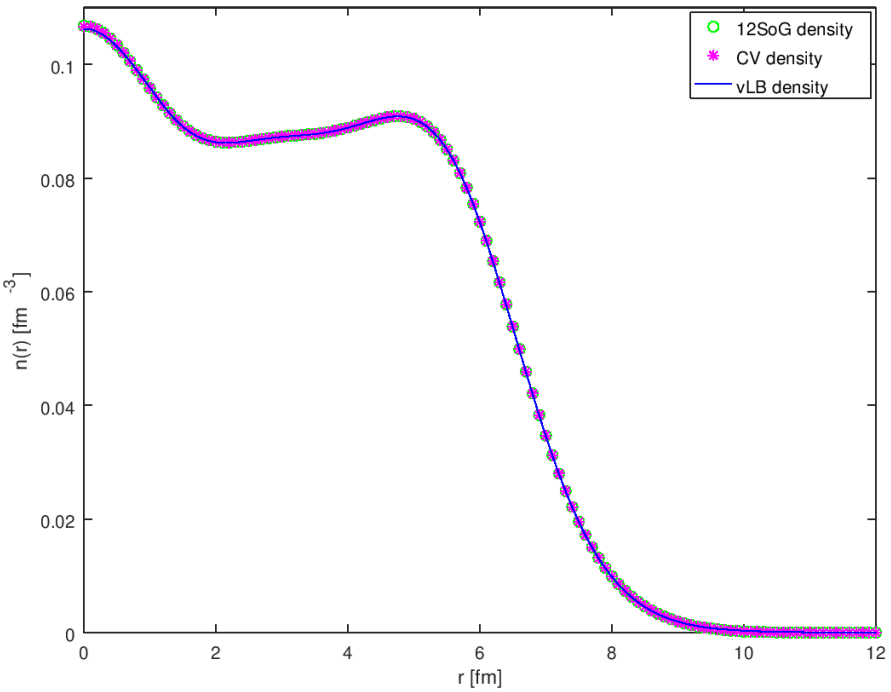

Figure 5.21: Comparison between the vLB density (continuous line), CV density (asterisk) and SoG density (rings) for ^{208}Pb neutrons case.

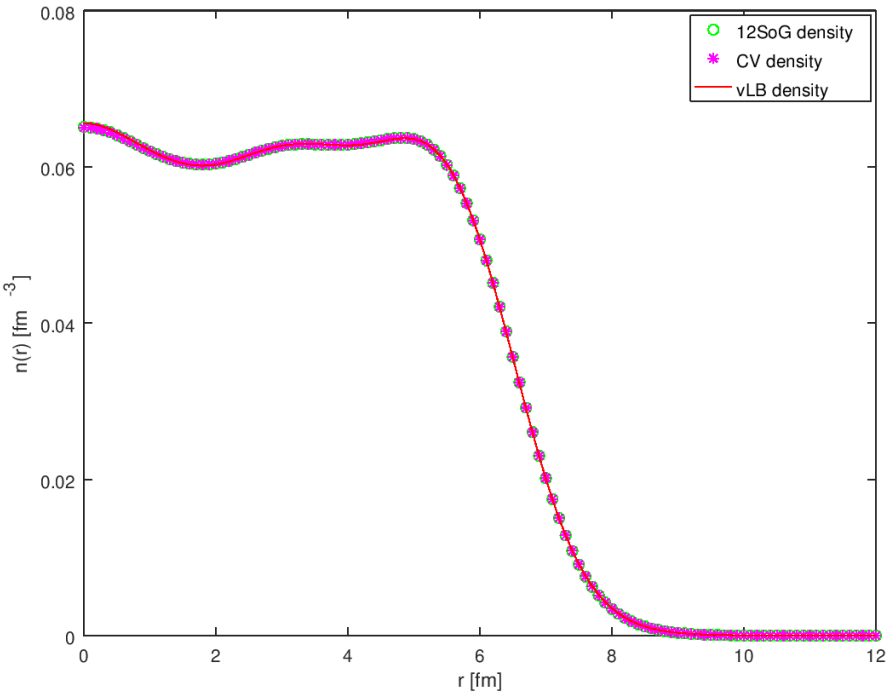

Figure 5.22: Comparison between the vLB density (continuous line), CV density (asterisk) and SoG density (rings) for ^{208}Pb protons case.

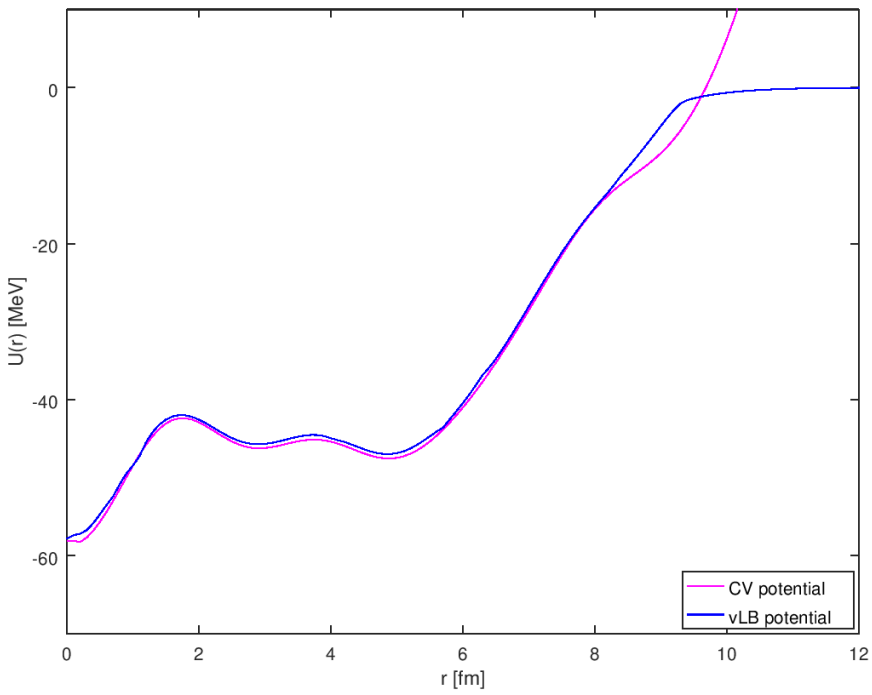

Figure 5.23: Comparison between the vLB and CV potentials obtained with SoG density target for ^{208}Pb neutrons case. CV potential has been shifted down $9MeV$.

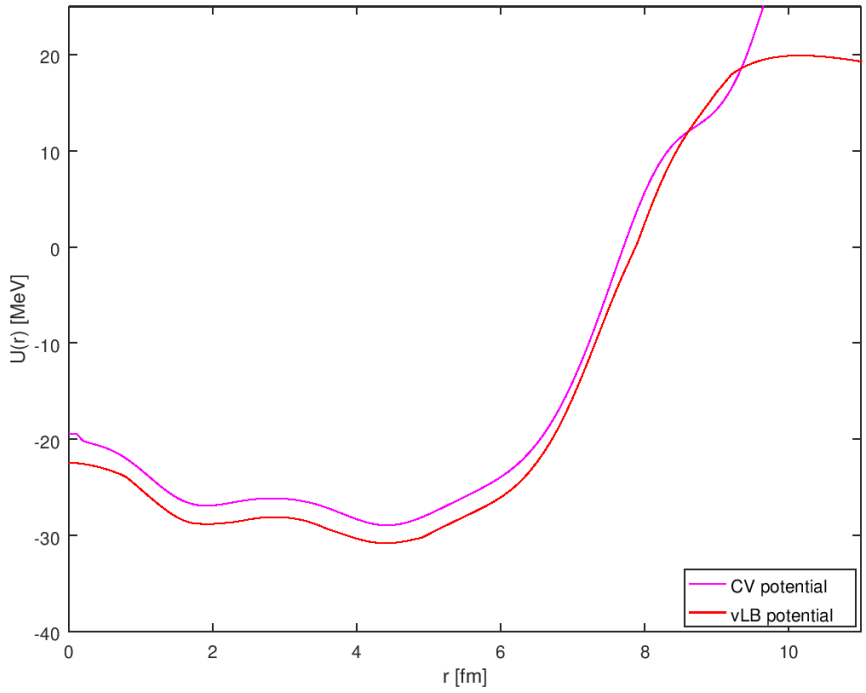

Figure 5.24: Comparison between the vLB and CV potentials obtained with SoG density target for ^{208}Pb protons case.

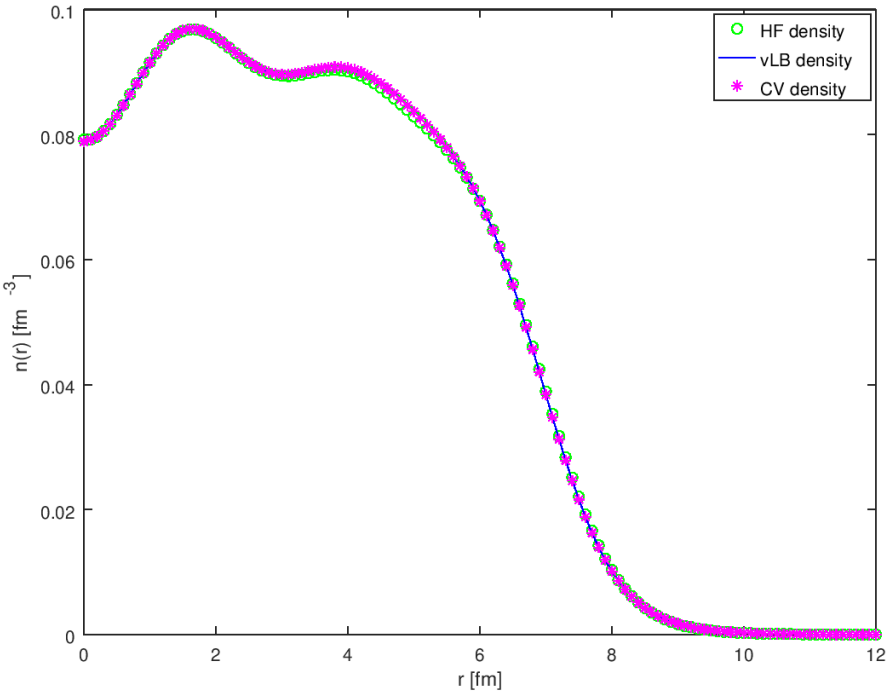

Figure 5.25: Comparison between the vLB density (continuous line), CV density (asterisk) and HF density (rings) for ^{208}Pb neutrons case.

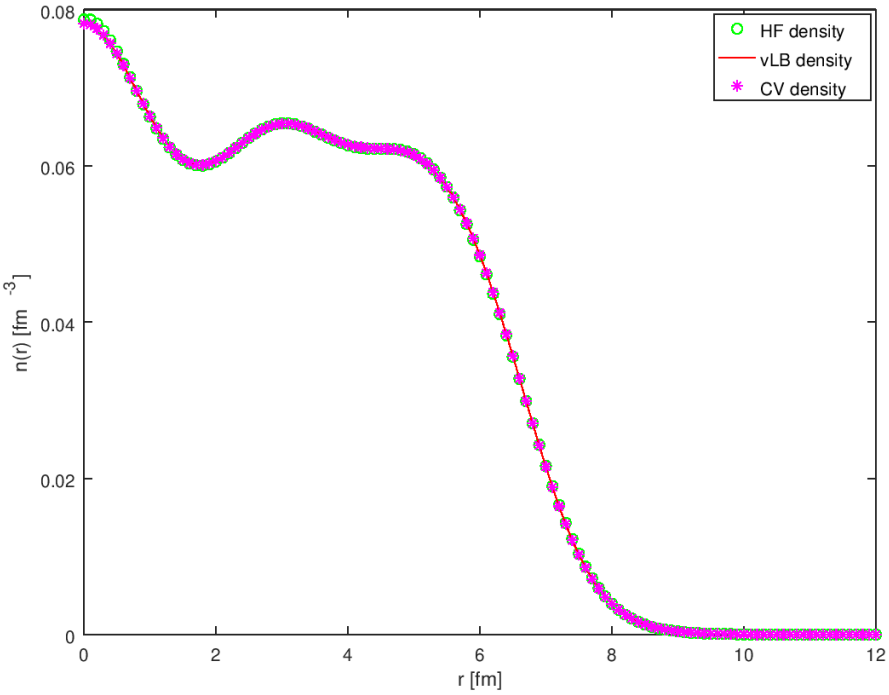

Figure 5.26: Comparison between the vLB density (continuous line), CV density (asterisk) and HF density (rings) for ^{208}Pb protons case.

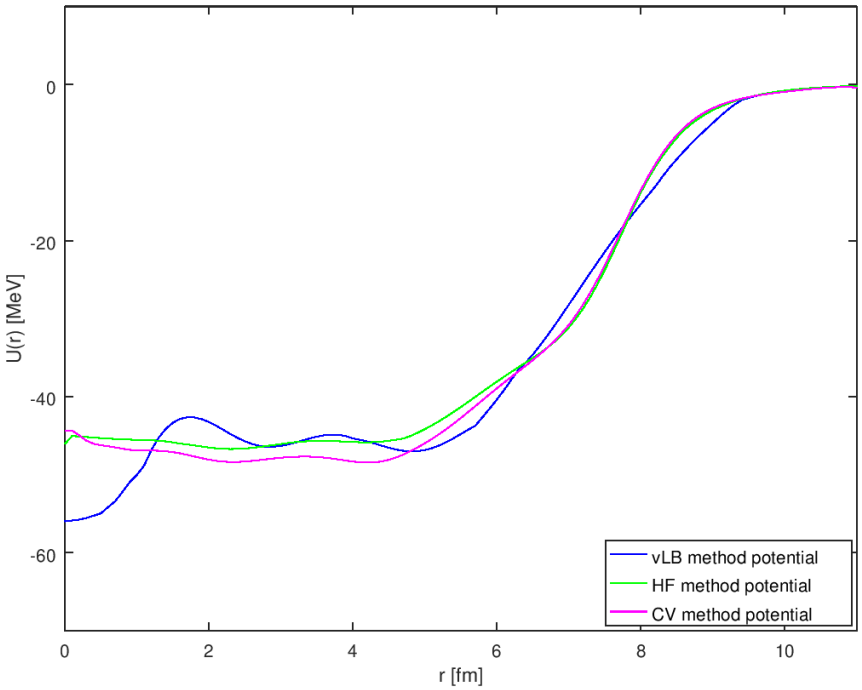

Figure 5.27: Comparison between the vLB, CV and HF potentials obtained with HF density target for ^{208}Pb neutrons case.

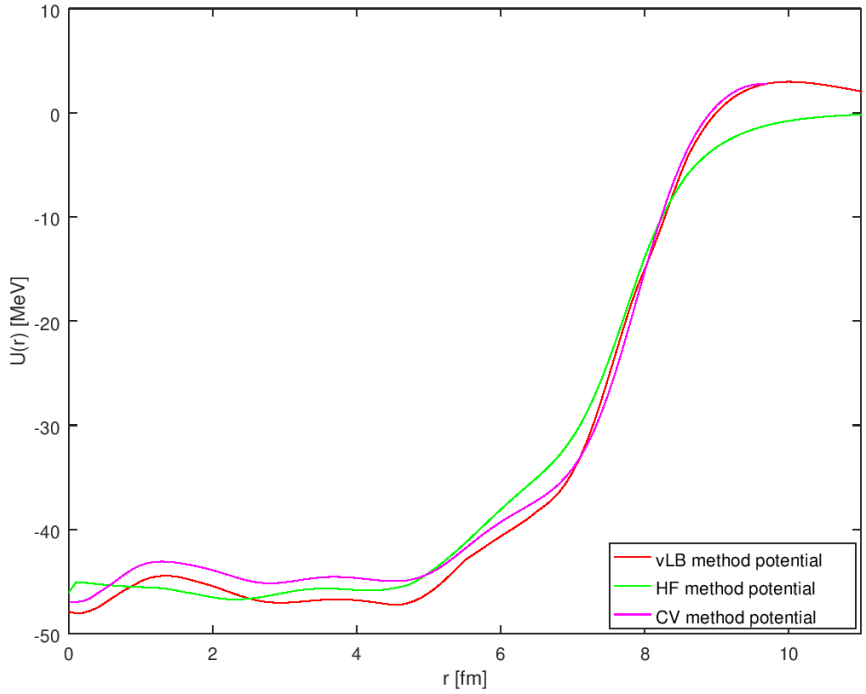

Figure 5.28: Comparison between the vLB, CV and HF potentials obtained with HF density target for ^{208}Pb protons case. CV and vLB potentials have been shifted down $17MeV$.

Chapter 6

Conclusion

The density functional theory, successfully developed for atoms, molecules, solids, only in the last decades has found place in the field of nuclear physics. This represents the most obvious alternative to the already tested Hartree-Fock theory and try to remedy to the limitations of this latter. The literature also witnesses many approach towards solving the nuclear direct Kohn-Sham problem, but the treatment of the nuclear inverse problem is totally missing.

The following thesis project has set the objective of contributing, together with other works, to the prediction of nuclear potentials starting from the experimental density.

The first step consisted in the inversion of the Kohn-Sham equations [6] adopting the inversion algorithm proposed by van Leeuwen and Baerends [7]. Particular attention was paid to the implementation of the mathematical model under study, to leave to the Milan group a code with a clean and modular architecture. Having taken as reference three doubly magical nuclei, ^{16}O, ^{40}Ca and ^{208}Pb, by several changes of the initial parameters we tried to evaluate the robustness of the algorithm inversion and detecting its limitations. The densities obtained from the solution of the direct problem follow, aside from than small imperfections, the experimental ones. The potentials associated with them, have very clear numerical noise for the ^{16}O (representing the light nuclei) which is less evident in medium-size nuclei. The best results were obtained for ^{208}Pb, with completely clean tails. This highlights how the vLB scheme finds its best performance for high systems with smaller surface-to-volume ratios.

Subsequently, the initial data was modified. Through small variations of the parameters to the initial Woods-Saxon potential, no particular anomalies were found. Only by increasing the depth of initial potential, the non-convergence of the iterative process has been achieved. The use of the harmonic oscillator potential as an initial potential has led to an excessive increase in numerical anomalies and a greater

difficulty in finding convergence. From this point of view, the vLB method proves very sensitive to the initial data. The origin of its limits can be found in the convergence condition. This represents a delicate element in the iterative scheme whose attempts at modification were not trivial and unsuccessful.
Finally, a comparison was made with the densities and potentials obtained from other predictive method, the Variational Constraint method and the Hartree-Fock method. Once again, the results obtained were in agreement with the analogues predicted by CV and HF. In particular, the comparison between the vLB method and the CV method, shows how the first always brings the potential tails to zero, while the second undergoes the asymptotic behavior of the SoG parametrization.
The present work is part of an exploratory investigation that still offers many possibilities for improvement. The inversion algorithm vLB, simple to implement but undoubtedly limited, can however make its contribution. In the future, it may be useful to make the vLB inversion scheme work together with the CV scheme in a synergic way, to implement a more robust and accurate predictive model.

Appendix A

Deconvolution from Proton Charge Density to Proton Density

In most experiments conducted for the study of nuclear matter, charged particles are used as probes. In particular, electron beams are used and these interact only with the protons of the nuclei under examination. Therefore, the result obtained is a charge density relative to protons only. In this work, it was necessary to know the particle distribution density obtained from the experimental charge density distribution. Afterwards, the idea that has allowed us to satisfy this need is shown in greater detail.
The charge density $n_{ch}(r)$ is related to the density of protons $n_p(r)$ by a convolution

$$n_{ch} = [F_p(r - r') * n_p(r')](r) = \int dr'[F_p(r - r') * n_p(r')](r) \tag{A.1}$$

where $F_p(r - r')$ is the proton form factor with respect to the electric force. This quantity represents the shape of the proton, which is not considered a point. The form factor must be normalized to the proton charge q_e. To obtain $n_p(r)$, a deconvolution of the (A.1) is necessary and it is convenient to pass in the momentum space, where the two densities are linked by a Fourier transform

$$\widehat{n}_{ch}(q) = \widehat{F}_p(q)\widehat{n}_p(q) \tag{A.2}$$

Via a backward Fourier transformation, one get

$$n_p(r) = (\widehat{n}_p(q))^{\vee} \tag{A.3}$$

Considering a charge density given by a sum of Gaussians

$$n_{ch}(r) = \sum_i \frac{A_i}{2\pi^{\frac{3}{2}}\gamma^3}[e^{\frac{(r-R_i)^2}{\gamma^2}} + e^{\frac{(r+R_i)^2}{\gamma^2}}], \tag{A.4}$$

where

$$A_i = \frac{q_e Z Q_i}{1 + 2\frac{R_i^2}{2}} \tag{A.5}$$

Z is the atomic number of the nucleus, γ is a width parameter proportional to the rms radius of the nucleus, whereas R_i and Q_i[1] are parameters.
In spherical symmetry, the Fourier transform takes the shape

$$\widehat{f}(q) = 4\pi \int_0^\infty r dr \frac{sin(q,r)}{q} f(r) \tag{A.6}$$

and the anti-trasformation is

$$\check{f}(q) = \frac{1}{2\pi^2 r} \int_0^\infty q dq \frac{sin(q,r)}{r} f(q) \tag{A.7}$$

Then, the Fourier transform of the (A.1) can be written as

$$\begin{aligned} \widehat{n}_{ch}(q) &= 4\pi \int_0^\infty dr \frac{sin(q,r)}{q} n_{ch}(r) \\ &= \sum_i \frac{4\pi}{q} \frac{A_i}{2\pi^{\frac{3}{2}}\gamma^3} \int_0^\infty r dr sin(qr)[e^{\frac{(r-R_i)^2}{\gamma^2}} + e^{\frac{(r+R_i)^2}{\gamma^2}}] \\ &\quad - \sum_i \frac{A_i}{2q} \frac{\partial q}{\sqrt{\pi}\gamma^2} \int_{-\infty}^\infty du[e^{iq(\gamma u \mp R_i} + e^{-iq(\gamma u \mp R_i}] \\ &= \sum_i A_i e^{-\frac{q^2\gamma^2}{4}}[cos(qR_i) + \frac{2R_i}{q\gamma^2} sin(qR_i)] \end{aligned} \tag{A.8}$$

From [38] it is possible to define the Gaussian form factor for the proton

[1] It must satisfy the condition $\sum_i Q_i = 1$

$$F_p(r-r') = \frac{qr}{\pi^{\frac{3}{2}}\alpha^3} e^{-\frac{(r-r')^2}{\alpha^2}}, \tag{A.9}$$

where α is proportional to the root mean squared radius of the proton. By Furier trasformation of form factor, one get

$$\widehat{F}_p(q) = q_e e^{-\frac{q^2\alpha^2}{4}} \tag{A.10}$$

Now, with $\beta^2 = \gamma^2 - \alpha^2$, the deconvolution can be calculated

$$\widehat{n}_p(q) = \sum_i \frac{A_i}{q_e} e^{-\frac{q^2\beta^2}{4}} [cos(qR_i) + \frac{2R_i}{q\gamma^2} sin(qR_i)] \tag{A.11}$$

Finally, the inverse Fourier transform for nuclear density can be calculated. For simplicity, the steps for the sine and cosine terms are shown separately. For the cosine term, one get

$$\begin{aligned} n_{pI}(r) &= \sum_i \frac{A_i}{q_e} \frac{1}{2\pi^2 r} \int_0^\infty q dq \frac{sin(q,r)}{r} cos(qR_i) e^{-\frac{q^2\beta^2}{4}} \\ &= \sum_i \frac{A_i}{16 q_e \pi^2 r} \partial_r \int_{-\infty}^{\infty} dq [e^{iq(r+R_i)} + e^{-iq(r+R_i)} + e^{iq(r-R_i)} + e^{-iq(r-R_i)}] e^{-\frac{q^2\beta^2}{4}} \\ &= \sum_i \frac{A_i}{2 q_e \pi^{\frac{3}{2}} \beta^3 r} [(r+R_i) e^{-\frac{(r+R_i)^2}{\beta^2}} + (r-R_i) e^{-\frac{(r-R_i)^2}{\beta^2}}]. \end{aligned} \tag{A.12}$$

For the sine term, give

$$\begin{aligned} n_{pII}(r) &= \sum_i \frac{A_i R_i}{q_e \gamma^2} \frac{1}{2\pi^2 r} \int_0^\infty q dq \frac{sin(q,r)}{r} sin(qR_i) e^{-\frac{q^2\beta^2}{4}} \\ &= \sum_i \frac{A_i R_i}{2 q_e \pi^2 \gamma^2 r} \int_{-\infty}^{\infty} dq \frac{e^{iqr} - e^{-iqr}}{2i} \frac{e^{iqR_i} - e^{-iqR_i}}{2i} e^{-\frac{q^2\beta^2}{4}} \\ &= \sum_i \frac{A_i R_i}{2 q_e \pi^{\frac{3}{2}} \gamma^2 \beta r} [e^{-\frac{(r-R_i)^2}{\beta^2}} - e^{-\frac{(r+R_i)^2}{\beta^2}}] \end{aligned} \tag{A.13}$$

Joining the two contributions gives the result

$$n_p(r) = \sum_i \frac{A_i}{2 q_e \pi^{\frac{3}{2}} \beta r} [(\frac{r-R_i}{\beta^2} + \frac{R_i}{\gamma^2}) e^{-\frac{(r-R_i)^2}{\beta^2}} + (\frac{r+R_i}{\beta^2} - \frac{R_i}{\gamma^2}) e^{-\frac{(r+R_i)^2}{\beta^2}}]. \tag{A.14}$$

Bibliography

[1] D. Vautherin and D.M. Brink. Hartree-fock calculations with skyrme's interaction. i. spherical nuclei. *Physical Review C*, 5(3):626–647, 1972.

[2] T.H.R. Skyrme. Cvii. the nuclear surface. *Philosophical Magazine*, 1(11):1043–1054, 1956.

[3] J. Decharg and D. Gogny. Hartree-fock-bogolyubov calculations with the d 1 effective interaction on spherical nuclei. *Physical Review C*, 21(4):1568–1593, 1980.

[4] G. Coló. Density functional theory (dft) for atomic nuclei: a simple introduction. *arXiv:1807.02643v1[nucl-th]*, 7 Jul. 2018.

[5] R. Nityananda, P. Hohenberg, and W. Kohn. Inhomogeneous electron gas. *Resonance*, 22(8):809–811, 2017.

[6] W. Kohn and L.J. Sham. Self-consistent equations including exchange and correlation effects. *Physical Review*, 140(4A):A1133–A1138, 1965.

[7] R. van Leeuwen and E.J. Baerends. Exchange-correlation potential with correct asymptotic behavior. *Physical Review A*, 49(4):2421–2431, 1994.

[8] D.S. Jensen and A. Wasserman. Numerical methods for the inverse problem of density functional theory. *International Journal of Quantum Chemistry*, 118(1), 2018.

[9] H. De Vries, C.W. De Jager, and C. De Vries. Nuclear charge-density-distribution parameters from elastic electron scattering. *Atomic Data and Nuclear Data Tables*, 36(3):495–536, 1987.

[10] J. Zenihiro, H. Sakaguchi, T. Murakami, M. Yosoi, Y. Yasuda, S. Terashima, Y. Iwao, H. Takeda, M. Itoh, H.P. Yoshida, and M. Uchida. Neutron density distributions of 204,206,208pb deduced via proton elastic scattering at ep = 295 mev. *Physical Review C - Nuclear Physics*, 82(4), 2010.

[11] N. Schwierz, I. Wiedenhover, and A. Volya. Parameterization of the woods-saxon potential for shell-model calculations. *arXiv:0709.3525v1[nucl-th]*, 21 Sep. 2007.

[12] Petrat Sören. Hartree corrections in a mean-field limit for fermions with coulomb interaction. *arXiv:1609.04754v2[math-ph]*, 24 May 2017.

[13] E. Caurier, G. Martinez-Pinedo, F. Nowacki, A. Poves, and A. P. Zuker. The shell model as unified view of nuclear structure. *arXiv:nucl-th/0402046v1*, 13 Feb. 2004.

[14] J. Holt and G. Brown. Hans bethe: The nuclear many body problem. *arXiv:nucl-th/0509016v1*, 7 Sep. 2005.

[15] M. Daene, A. Gonis, D. M. Nicholson, and G. M. Stocks. Solving the self-interaction problem in kohn-sham density functional theory: Application to atoms. *Journal of Physics and Chemistry of Solids*, 30 Apr. 2013.

[16] R. Anni, C. Co', and P. Pellegrino. Nuclear charge density distributions from elastic electron scattering data. *arXiv:nucl-th/9410023v1*, 17 Oct. 1994.

[17] T.L. Beck. Real-space mesh techniques in density-functional theory. *Reviews of Modern Physics*, 72(4):1041–1080, 2000.

[18] M.R. Pahlavani and S.A. Alavi. Solutions of woods-saxon potential with spin-orbit and centrifugal terms through nikiforov-uvarov method. *Communications in Theoretical Physics*, 58(5):739–743, 2012.

[19] M. Bender, P.-H. Heenen, and P.-G. Reinhard. Self-consistent mean-field models for nuclear structure. *Reviews of Modern Physics*, 75(1):121–180, 2003.

[20] F. Salvat, A. Jablonski, and C.J. Powell. Elsepa - dirac partial-wave calculation of elastic scattering of electrons and positrons by atoms, positive ions and molecules. *Computer Physics Communications*, 165(2):157–190, 2005.

[21] j. C. Slater. A semplification of the hartree-fock method. *Physical Review*, 81(3):385–390, 1951.

[22] Z. Romanowski. Numerical solution of kohn-sham equation for atom. volume 38, pages 3263–3286, 2007.

[23] R.D. Woods and D.S. Saxon. Diffuse surface optical model for nucleon-nuclei scattering [19]. *Physical Review*, 95(2):577–578, 1954.

[24] Md. Mizanur Rahman, Mst. Jesmin Ara, Md. Nurul Islam, and Md. Shajib Ali. Numerical study on the boundary value problem by using a shooting method. *Pure and Applied Mathematics Journal*, pages 96–100, 25 May 2015.

[25] D.J. Jones. Use of a shooting method to compute eigenvalues of fourth-order two-point boundary value problems. *Journal of Computational and Applied Mathematics*, 47(3):395–400, 1993.

[26] A. Campi. Private communications.

[27] S. Mayers. *Programmazione C++ moderna*. Hoepli, 2015.

[28] W. H. Press, W. T. Teukolsky, S. A.and Wetterling, and B. P. Flannery. *Numerical recipes*. Cambridge University Press, third edition, 2007.

[29] P. Ring and P. Schuck. *The Nuclear Many-Body Problem*. Springer, 1980.

[30] N. Zettili. *Quantum Mechanics*. Wiley, second edition, 2009.

[31] A. Bohr and B. R. Mottelson. *Nuclear Structure*, volume 1. World Scientific, 1998.

[32] G. Accorto. *A Constrained-Minimization Method for the Solution of the Inverse Kohn-Sham Problem in Nuclei*. Master Thesis Not Published, 2018.

[33] A. Porro. *Potenziali nucleari da densit e distribuzioni di spin microscopiche*. Bachelor Thesis Not Published, 2017.

[34] X. N. Martinez Cuenca. *Deduzione di potenziale medio e massa efficace dei nucleoni dalle densit nucleari*. Bachelor Thesis Not Published, 2018.

[35] I. Macocco. *Costruzione del potenziale nucleare ecace di Kohn-Sham dalle densit empiriche*. Bachelor Thesis Not Published, 2017.

[36] J.C. Slater. A simplification of the hartree-fock method. *Physical Review*, 81(3):385–390, 1951. cited By 2967.

[37] D. Brink and E. Boeker. Nuclear physics a. 91, 1967.

[38] Z. Ye, J. Arrington, R.J. Hill, and G. Lee. Proton and neutron electromagnetic form factors and uncertainties. *Physics Letters, Section B: Nuclear, Elementary Particle and High-Energy Physics*, 777:8–15, 2018. cited By 5.